JOURNAL OF GEOPHYSICAL RESEARCH, VOL. 99, NO. D11, PAGES 22,831–22,855, NOVEMBER 20, 1994

Evidence for interannual variability of the carbon cycle from the National Oceanic and Atmospheric Administration/Climate Monitoring and Diagnostics Laboratory Global Air Sampling Network

Thomas J. Conway, Pieter P. Tans, Lee S. Waterman, and Kirk W. Thoning

National Oceanic and Atmospheric Administration, Climate Monitoring and Diagnostics Laboratory, Boulder, Colorado

Duane R. Kitzis, Kenneth A. Masarie, and Ni Zhang

Cooperative Institute for Research in Environmental Sciences, University of Colorado, Boulder

Abstract. The distribution and variations of atmospheric CO_2 from 1981 to 1992 were determined by measuring CO_2 mixing ratios in samples collected weekly at a cooperative global air sampling network. The results constitute the most geographically extensive, carefully calibrated, internally consistent CO_2 data set available. Analysis of the data reveals that the global CO_2 growth rate has declined from a peak of ~2.5 ppm yr^{-1} in 1987-1988 to ~0.6 ppm yr^{-1} in 1992. In 1992 we find no increase in atmospheric CO_2 from 30° to 90°N. Variations in fossil fuel CO_2 emissions cannot explain this result. The north pole-south pole CO_2 difference increased from ~3 ppm during 1981-1987 to ~4 ppm during 1988-1991. In 1992 the difference was again ~3 ppm. A two-dimensional model analysis of the data indicates that the low CO_2 growth rate in 1992 is mainly due to an increase in the northern hemisphere CO_2 sink from 3.9 Gt C yr^{-1} in 1991 to 5.0 Gt C yr^{-1} in 1992. The increase in the north pole-south pole CO_2 difference appears to result from an increase in the southern hemisphere CO_2 sink from ~0.5 to ~1.5 Gt C yr^{-1}.

Introduction

From 1980 to 1990 the anthropogenic increase in atmospheric carbon dioxide (CO_2) accounted for 55% of the change in radiative forcing due to all greenhouse gas emissions [*Intergovernmental Panel on Climate Change (IPCC)*, 1990]. The recently observed decline in the growth rate of chlorofluorocarbons in the troposphere [*Elkins et al.*, 1993] and recent results showing that stabilization of atmospheric methane would require relatively modest and achievable reductions in anthropogenic sources [*Hogan et al.*, 1991; *Steele et al.*, 1992; *Dlugokencky et al.*, 1994] will further shift the emphasis toward CO_2 as the primary agent of global climate change. The annual emissions of CO_2 from fossil fuel combustion, currently ~6 Gt C per year (Gt = 10^{15} g), continue to increase [*Marland and Boden*, 1991] and efforts to reduce or even stabilize CO_2 emissions will face huge political obstacles.

Predictions of future atmospheric CO_2 levels based on economic projections or extrapolation of current trends are complicated by our incomplete understanding of the global carbon cycle. Attempts to balance the global carbon budget based on atmospheric measurements [e.g., *Pearman and Hyson*, 1980; *Enting and Mansbridge*, 1989; *Tans et al.*, 1989] point to the existence of a northern hemisphere CO_2 sink of 3-4 Gt C, more than half of annual fossil fuel emissions. Note that carbon budgets based on surface CO_2 fluxes, which lead to the observed atmospheric CO_2 gradients are different from decadal-scale budgets based on where the carbon is eventually stored [*Tans et al.*, 1994]. A recent analysis of oceanic CO_2 measurements concluded that the ocean CO_2 sink in the northern hemisphere is at most 1 Gt C per year, in which case a balanced carbon budget would require a northern hemisphere terrestrial sink of 2-3 Gt C per year [*Tans et al.*, 1990]. Later refinements to this analysis included a correction for the cool skin of the ocean [*Robertson and Watson*, 1992], which added 0.4 Gt C to the global ocean sink, a correction for the transport of organic and inorganic C by rivers to the oceans, which added up to 0.5 Gt C to the ocean uptake [*Sarmiento and Sundquist*, 1992], and atmospheric oxidation of CO, which added 0.2 Gt C to the global ocean sink [*Enting and Mansbridge*, 1991]. The process mostly responsible for a large sink in the terrestrial ecosystems of the northern hemisphere has not yet been identified. In addition, it is known that the interannual variability in the carbon cycle related to natural climate fluctuations, e.g., El Niño/Southern Oscillation events, can be relatively large compared to annual fossil fuel emissions [e.g., *Bacastow*, 1976; *Gaudry et al.*, 1987]. The processes and feedbacks connecting climate and the carbon cycle are very poorly understood but are almost certain to be perturbed by any CO_2-induced climate change, further complicating attempts to predict the climatic consequences of increasing CO_2.

Since the atmosphere integrates the signals from all sources and sinks, measurements of the spatial and temporal variations of atmospheric CO_2 can be used to estimate sources and sinks [*Tans et al.*, 1989; *Enting and Mansbridge*, 1989; *Keeling et al.*, 1989a] and constrain carbon cycle model results [*Fung et al.*, 1983; *Pearman and Hyson*, 1986, *Potter et al.*, 1993]. The National Oceanic and Atmospheric Administration's Climate Monitoring and Diagnostics Laboratory (NOAA/CMDL) has

Paper number 94JD01951.
0148-0227/94/94JD-01951$05.00

measured CO_2 at a global network of sites since the late 1970s [*Komhyr et al.*, 1985; *Conway et al.*, 1988]. In this paper we present the results from 1981 to 1992, thus extending our previously published results by 8 years and including results from several new sampling locations. These measurements constitute the most geographically extensive, carefully calibrated, internally consistent atmospheric CO_2 data set available.

Analysis of these data reveals several significant results: an overall decline in the global atmospheric CO_2 growth rate from a peak in 1987-1988 through 1992; an extremely small increase in atmospheric CO_2 during 1991-1992, particularly in the northern hemisphere; and significant interannual variations in the interhemispheric gradient of atmospheric CO_2.

We also present results from an inversion of the data using a two-dimensional transport model [*Tans et al.*, 1989] to investigate the spatial and temporal variations in sources and sinks required to produce the observed latitudinal atmospheric CO_2 distribution.

Experimental Methods

The method of collecting air samples in glass flasks and measuring CO_2 mixing ratios by nondispersive infrared analysis has been described previously [*Komhyr et al.*, 1983; *Conway et al.*, 1988]. These same basic methods were used to obtain the data presented in this paper, but the flasks, the sample collection equipment, the analytical apparatus, and the network itself have all been improved, as described below.

Starting in 1968, the NOAA/CMDL flask project has primarily used 0.5-L Pyrex glass flasks tapered at both ends to ground glass stopcocks lubricated with a hydrocarbon grease (Apiezon N). Although the greased stopcocks were relatively effective, they became difficult to open and to close at cold temperatures, the stopcocks required frequent maintenance (regreasing and regrinding), and grease crept into the flasks necessitating a time-consuming cleaning and annealing process. The most important drawback to the greased stopcocks became apparent after we began measuring additional species in the flasks in 1983 and 1988 [*Steele et al.*, 1987; *Novelli et al.*, 1992]. Laboratory tests showed that CH_4 was stable in the greased flasks, but carbon monoxide was not. Thus although it was analytically feasible to measure CO by gas chromatography as we were doing for CH_4, mixing ratios of CO were observed to increase in the flasks over time, presumably due to photooxidation of the hydrocarbon grease. After testing many possible alternatives, we began using 0.5-L flasks equipped with glass piston Teflon O-ring stopcocks (J. Young, Acton, United Kingdom) in 1989. These flasks produced no change in CO mixing ratios for storage times up to 3 weeks [*Novelli et al.*, 1992].

In 1990 we began a program to measure the isotopic ratios $^{13}C/^{12}C$ and $^{18}O/^{16}O$ of CO_2 in the gas remaining in the flasks after CH_4, CO, and CO_2 had been measured. To obtain sufficient sample for the mass spectrometer, it was necessary to combine the residual air from both members of a 0.5-L flask pair. Comparisons with isotopic measurements from samples collected in larger flasks showed decreased scatter (improved precision) when larger volumes were used. In addition, larger volume flasks were found to be stable for CO over longer storage times [*Novelli et al.*, 1992]. Therefore in 1991 we began using 2.5-L glass flasks equipped with two Teflon O-ring (J. Young or Glass Expansion, Melbourne, Australia) stopcocks. To ensure that the flask is thoroughly flushed during sampling, these flasks have a diptube connected to the inlet stopcock, which reaches to the bottom of the flask.

All the modifications to the flask design were tested extensively in the laboratory to ensure that the mixing ratios of CO_2, CH_4, and CO were stable in the flasks. Also, when the flasks were deployed to the network, sampling was conducted in an overlap mode at many sites for several months. The results from overlapped sampling showed convincingly that no offsets or biases were introduced into the data.

Since 1981, flask samples were collected using a portable, battery-powered pumping unit described by *Komhyr et al.* [1985]. In mid-1990 we began using a sampling unit based on the same flushing and pressurizing principles as the original sampler but with significant modifications. This sampler uses a single 12-V, 3.2-ampere-hour lead-acid battery to power a pump (Air Cadet) able to produce higher flow rates and pressures than the original pump. A back pressure regulator and valve arrangement are used to control the pressure in the flasks. A longer mast and intake line (5 m) are used to further decrease the possibility of sample contamination, either by the sample collector or by local surface vegetation. Finally, the case is larger to accommodate 2.5-L flasks and more rugged to better withstand repeated use in a variety of extreme environments. The current procedure with this sampler is to flush the 2.5-L flasks for 5 min at ~8 Lpm, and then pressurize them to 3-4 psig.

The positive effect of these flask and sampler improvements is shown in Figure 1. On the basis of laboratory experiments and the low atmospheric variability of CO_2 mixing ratios at remote locations, we expect that for a properly collected flask sample that does not leak between collection and analysis the CO_2 mixing ratio difference between members of a sample pair should be less than 0.5 ppm. Figure 1 shows the percentage of pairs meeting this criterion (good pairs) from all sites from 1987 to 1992. The percentage of good pairs has increased from ~75% in 1987-1988 to ~90% in 1992. We attribute most of this improvement to the elimination of grease from the flasks. The overlapped sampling revealed that at humid tropical sites the percentage of good pairs increased significantly with Teflon O-ring flasks. The improvement was less at cooler, drier sites. A final factor relating to improved sample quality is an increased emphasis on face-to-face training. Whenever possible, new sample collectors visit Boulder for 1-2 days of training before collecting samples in the field. Occasionally, personnel from CMDL visit the sampling locations to conduct training and also to optimize the exact sample collection site. These activities have also contributed to the improved rate of successful sample collection.

Flask samples were analyzed since 1980 by nondispersive infrared analysis using the apparatus described by *Komhyr et al.* [1983]. In December of 1988 we began using a new analytical system (K.W. Thoning et al., Analysis system for measurement of the CO_2 mixing ratio in flask air samples, submitted to *Journal of Atmospheric and Oceanic Technology*, 1994). The new analytical system incorporates a Siemens Ultramat 3 nondispersive infrared analyzer. Sample transfer is accomplished with a KNF Neuberger pump. The main improvements with this design are better measurement reproducibility and an increase in sample throughput by a factor of 3. The analytical precision of this apparatus as determined by repeated measurements of flasks filled with gas from cylinders, or by measuring reference gas cylinders directly,

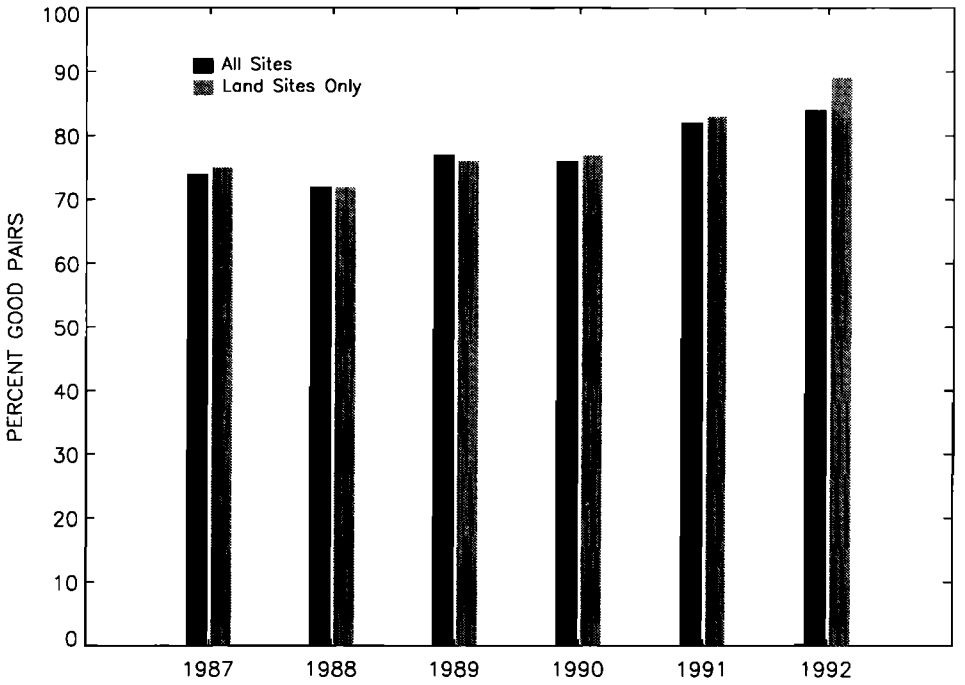

Figure 1. Annual percentages of flask sample pairs for which both members agree to within 0.5 ppm. The dark bar represents all sites, and the lighter bar excludes the shipboard samples that are not collected with the battery-powered sampler.

is ~0.05 ppm. All CMDL flask samples are measured relative to standards traceable to the World Meteorological Organization (WMO) Central CO_2 Laboratory operated by C. D. Keeling at the Scripps Institution of Oceanography [*Thoning et al.*, 1987]. The data reported here are in the WMO X85 mole fraction scale.

In this paper we present results from 32 land-based sampling sites shown in Figure 2 and listed in Table 1. Throughout this paper the three-letter codes given in Table 1 are used when referring to the sampling sites. Since sampling has been discontinued at Amsterdam Island (AMS) and St. Croix, Virgin Islands (AVI), 30 of the sites listed in Table 1 were active during 1992.

In adding sites to the network, we have attempted to improve our ability to deduce global and regional-scale source/sink patterns. We have increased our coverage of the remote marine boundary layer, e.g., Alert, Canada (ALT), Bermuda (east) (BME), Bermuda (west) (BMW), Sand Island, Midway (MID), and we have also been guided by three-dimensional tracer model results for both CO_2 and CH_4 [*Fung et al.*, 1983; *Fung et al.*, 1991] in choosing sites downwind from and closer to large source and sink regions, e.g., Shemya Island, Alaska (SHM) and Tae-ahn Peninsula, Korea (TAP). We have recently begun sampling continental interiors by choosing sites in desert regions, e.g., Qinghai Province, China (QPC), where the lack of local vegetation increases the probability of obtaining a sample of well-mixed, regionally representative air. The flask network data presented in this paper still primarily represent remote marine boundary layer air.

We have further increased our latitudinal coverage of the Pacific Ocean by sampling from container ships making regular voyages between Los Angeles and New Zealand, along the approximate tracks shown in Figure 2. This project began with cooperation from the Blue Star Line in 1987 on the *Southland Star*. Samples are collected at approximately 5° latitude intervals during southbound and northbound voyages, resulting in a sampling frequency of approximately one sample every 3 weeks per 5° latitude interval. In 1990 we began sampling on a second ship, the *Wellington Star*, thus increasing the sampling frequency to approximately one sample every 1.5 weeks per 5° interval. The shipboard samples are not collected with the portable pumping unit described above. Rather, they are collected in evacuated 3-L flasks that are filled sequentially by simply holding the flask into the wind, purging the dead volume in the inlet to the flask, opening the stopcock, and allowing the flask to fill with ambient air. This method is used for the convenience of the ship personnel and because it has been effectively used previously on ships where uncontaminated air can usually be sampled simply by choosing a location facing into the relative wind created by the moving ship.

Results

The CO_2 measurement results for flask samples collected at the flask network sites and in 14 latitude bands from shipboard sampling are presented in Figure 3 (a-tt). The individual flask measurements and monthly means for each site have been archived at the Carbon Dioxide Information Analysis Center, Oak Ridge National Laboratory, Oak Ridge, Tennessee; the World Data Center for Greenhouse Gases, Tokyo, Japan; and the National Climatic Data Center, Asheville, North Carolina. The data are also available directly from CMDL by accessing an ftp anonymous directory over Internet. The annual mean CO_2 mixing ratios calculated from the curve fits described below are given in Table 2.

Data Selection

The data selection methods used in this paper differ from our previous work [*Conway et al.*, 1988] in only two ways. First,

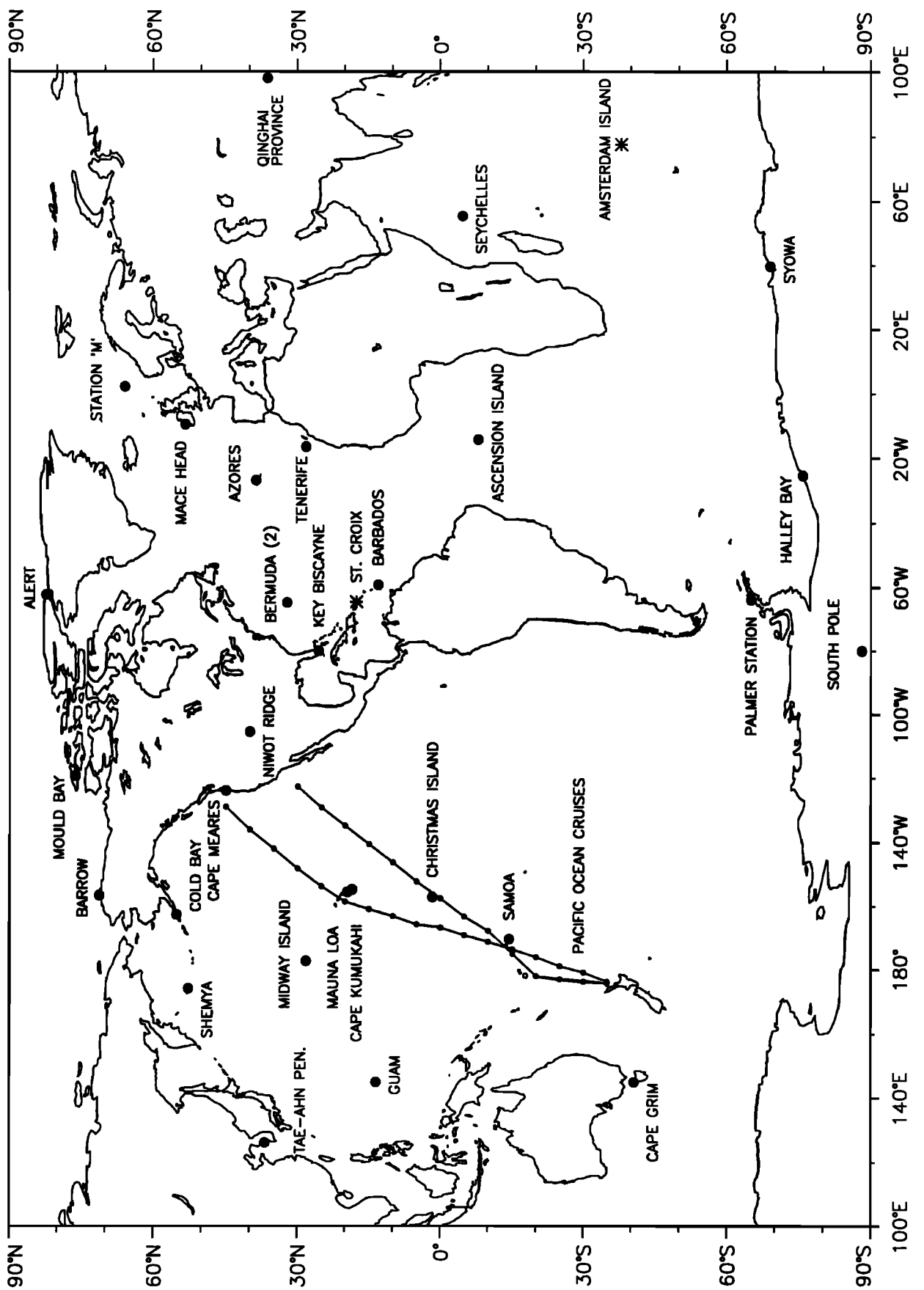

Figure 2. Map showing the locations of the Climate Monitoring and Diagnostic Laboratory (CMDL) cooperative flask-sampling network sites. The asterisks indicate sites where sampling has been discontinued.

Table 1. Summary of Flask Sampling Sites

Site Code	Site	Country	Latitude	Longitude	Elevation* m	Cooperating Agency	Site Type
ALT	Alert, Northwest Territories	Canada	82°27'N	62°31'W	210	Environment Canada/Atmospheric Environment Service	barren coastal hill
AMS	Amsterdam Island	France	37°57'S	77°32'E	150	Centre des Faibles Radioactivites	island seashore
ASC	Ascension Island	United Kingdom	7°55'S	14°25'W	54	USAF, Pan American World Airways	island seashore
AVI	St. Croix, Virgin Islands	United States	17°45'N	64°45'W	3	Fairleigh Dickinson University	island seashore
AZR	Terceira Island, Azores	Portugal	38°45'N	27°05'W	30	USAF/7th Weather Wing	air base
BME	St. David's Head	Bermuda	32°22'N	64°39'W	30	Atmosphere/Ocean Chemistry Experiment	rocky seashore
BMW	Southampton	Bermuda	32°16'N	65°53'W	30	Bermuda Biological Station	promontory seashore
BRW	Point Barrow, Alaska	United States	71°19'N	156°36'W	11	CMDL Observatory	Arctic coastal seashore
CBA	Cold Bay, Alaska	Unites States	55°12'N	162°43'W	25	NOAA/National Weather Service	treeless peninsula
CGO	Cape Grim, Tasmania	Australia	40°41'S	144°41'E	94	CSIRO, Division of Atmospheric Research	promontory seashore
CHR	Christmas Island	Kiribati	1°42'N	157°10'W	3	Scripps Institution of Oceanography	island seashore
CMO	Cape Meares, Oregon	United States	45°29'N	123°58'W	30	Oregon Graduate Institute of Science and Technology	promontory seashore
GMI	Guam, Mariana Islands	United States	13°26'N	144°47'E	2	University of Guam	island seashore

Table 1. (continued)

Site Code	Site	Country	Latitude	Longitude	Elevation* m	Cooperating Agency	Site Type
HBA	Halley Bay	Antarctica	75°40'S	25°30'W	10	British Antarctic Survey	barren seashore
IZO	Tenerife, Canary Islands	Spain	28°18'N	16°29'W	2300	Izaña Observatory/Spanish National Meteorological Institute	volcanic mountain
KEY	Key Biscayne, Florida	United States	25°40'N	80°12'W	3	NOAA/Atlantic Oceanographic and Meteorological Laboratory	coastal island seashore
KUM	Cape Kumukahi, Hawaii	United States	19°31'N	154°49'W	3	CMDL Site	island seashore
MBC	Mould Bay, Northwest. Territories	Canada	76°15'N	119°21'W	58	Environment Canada/ Atmospheric Environment Service	island tundra
MHT	Mace Head	Ireland	53°20'N	9°54'W	25	University College, Galway	island promontory
MID	Sand Island, Midway	United States	28°13'N	177°22'W	4	United States Navy/ITT	island seashore
MLO	Mauna Loa, Hawaii	United States	19°32'N	155°35'W	3397	CMDL Observatory	barren volcanic mountain slope
NWR	Niwot Ridge, Colorado	United States	40°03'N	105°38'W	3749	University of Colorado/ INSTAAR	alpine mountain
PSA	Palmer Station	Antarctica	64°55'S	64°00'W	10	National Science Foundation/ Antarctic Support Associates	barren island seashore
QPC	Qinghai Province	China	36°16'N	100°55'E	3810	Chinese Academy of Meteorological Sciences	semi dessert
RPB	Ragged Point	Barbados	13°10'N	59°26'W	3	International Science Consultants	island seashore

Table 1. (continued)

Site Code	Site	Country	Latitude	Longitude	Elevation* m	Cooperating Agency	Site Type
SEY	Mahé Island	Seychelles	4°40'S	55°10'E	3	New Mexico State University/ Physical Science Laboratory	island seashore
SHM	Shemya Island, Alaska	United States	52°43'N	174°06'E	40	USAF	barren island
SMO	American Samoa	United States	14°15'S	170°34'W	42	CMDL Observatory	island rocky promontory
SPO	South Pole Station	Antarctica	89°59'S	24°48'W	2810	CMDL Observatory/ National Science Foundation	ice and snow covered plateau
STM	Ocean Station "M"	Norway	66°00'N	2°00'E	7	Norway Meteorological Institute	open ocean
SYO	Syowa Station	Antarctica	69°00'S	39°35'E	11	Japanese Antarctic Research Expedition/National Institute for Polar Research	barren island seashore
TAP	Tae-ahn Peninsula	Republic of South Korea	36°44'N	126°08'E	20	Korea National University of Education	vegetated peninsula

USAF, United States Air Force; CMDL, Climate Monitoring and Diagnostics Laboratory; NOAA, National Oceanic and Atmospheric Administration; CSIRO, Commonwealth Scientific and Industrial Research Organization.

*Elevation above mean sea level.

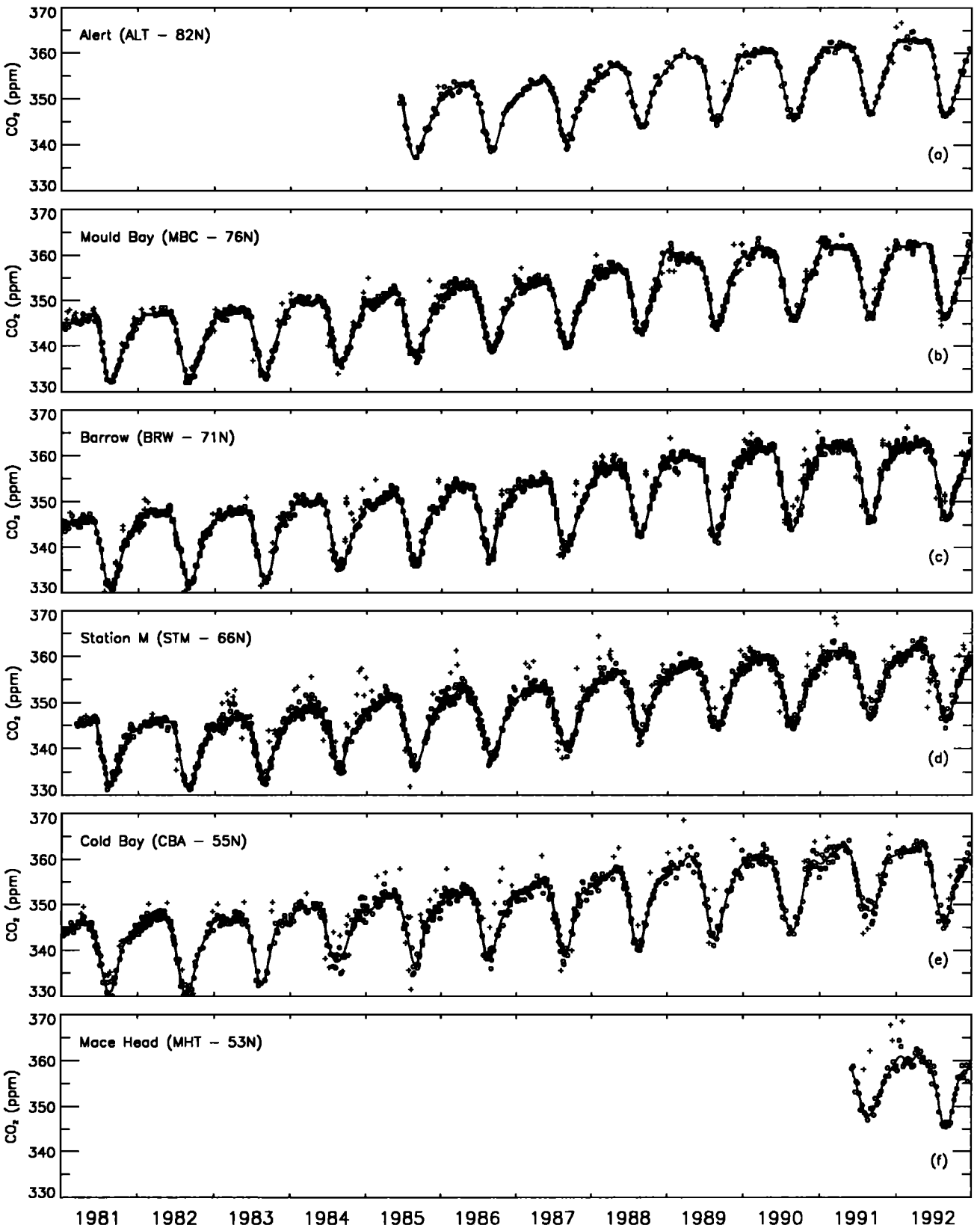

Figure 3. (a-tt) Flask sample CO_2 mixing ratios for the CMDL flask network sites. The open circles represent pair averages for samples meeting our selection criteria, as described in the text. The plus symbols represent samples determined to be valid measurements but not of well-mixed, regionally representative air. The solid curves, described in the text, are used for subsequent data analyses. Although the sizes of the plot frames vary, the absolute scale in part per million (ppm) per centimeter is the same for each site.

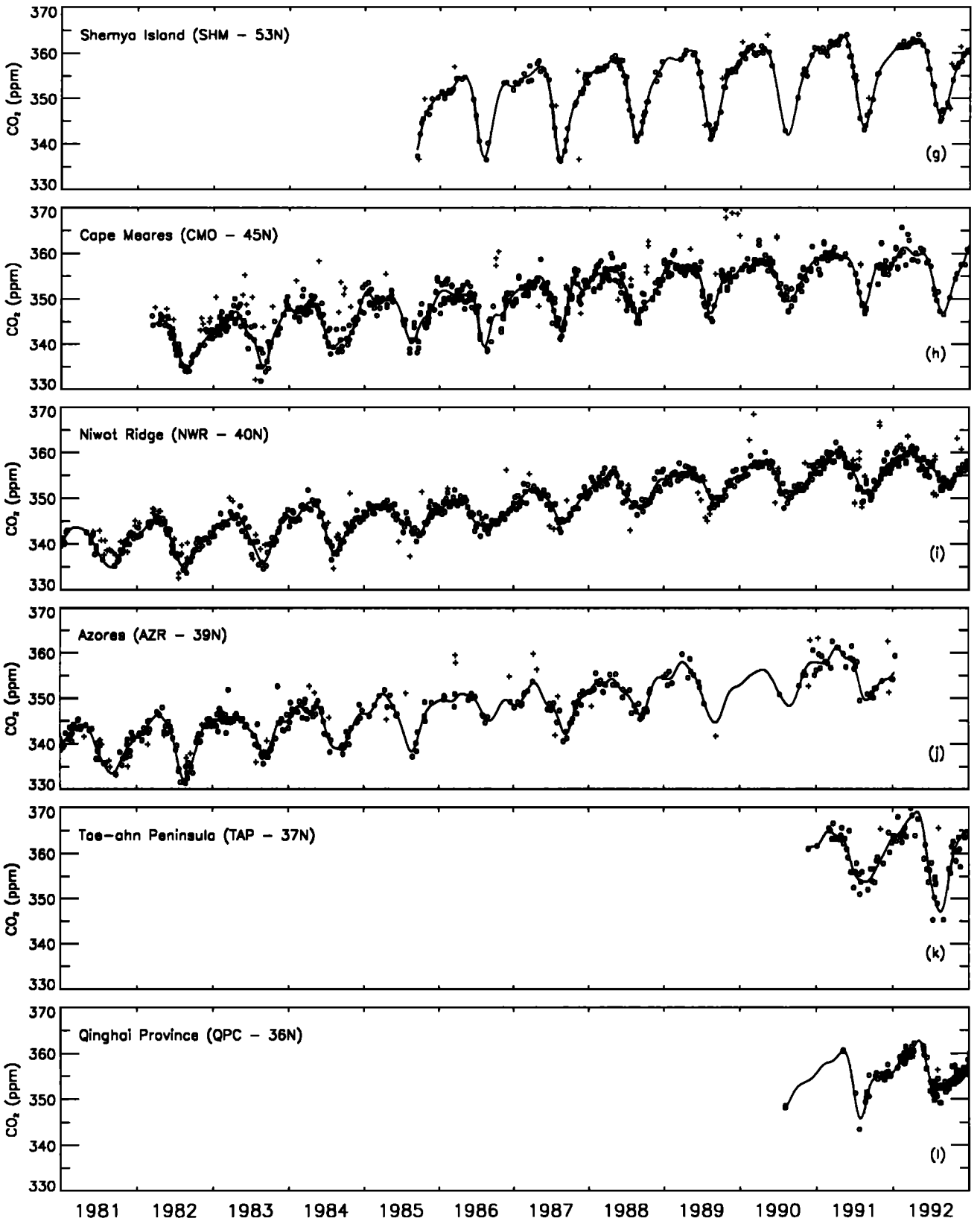

Figure 3. (continued)

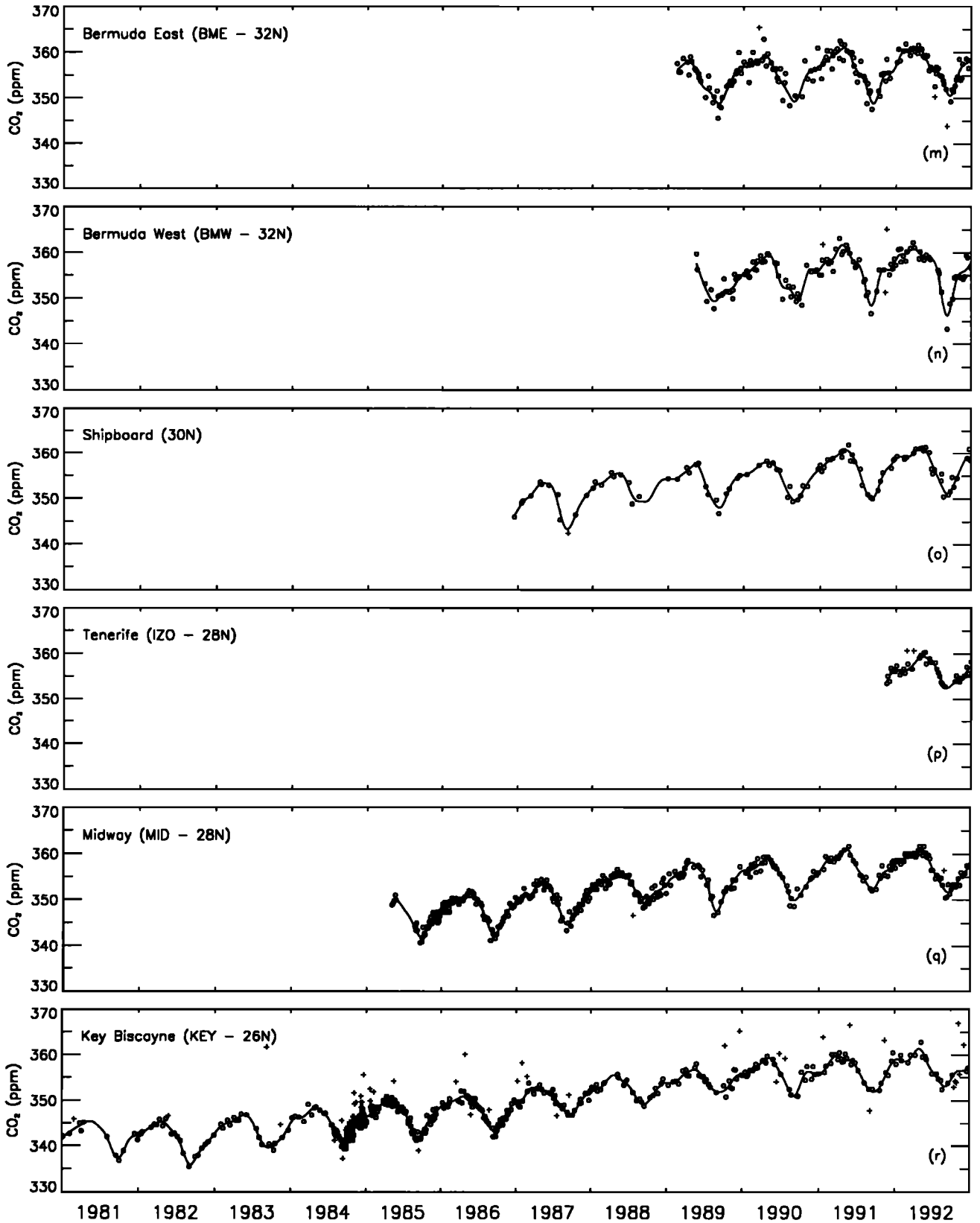

Figure 3. (continued)

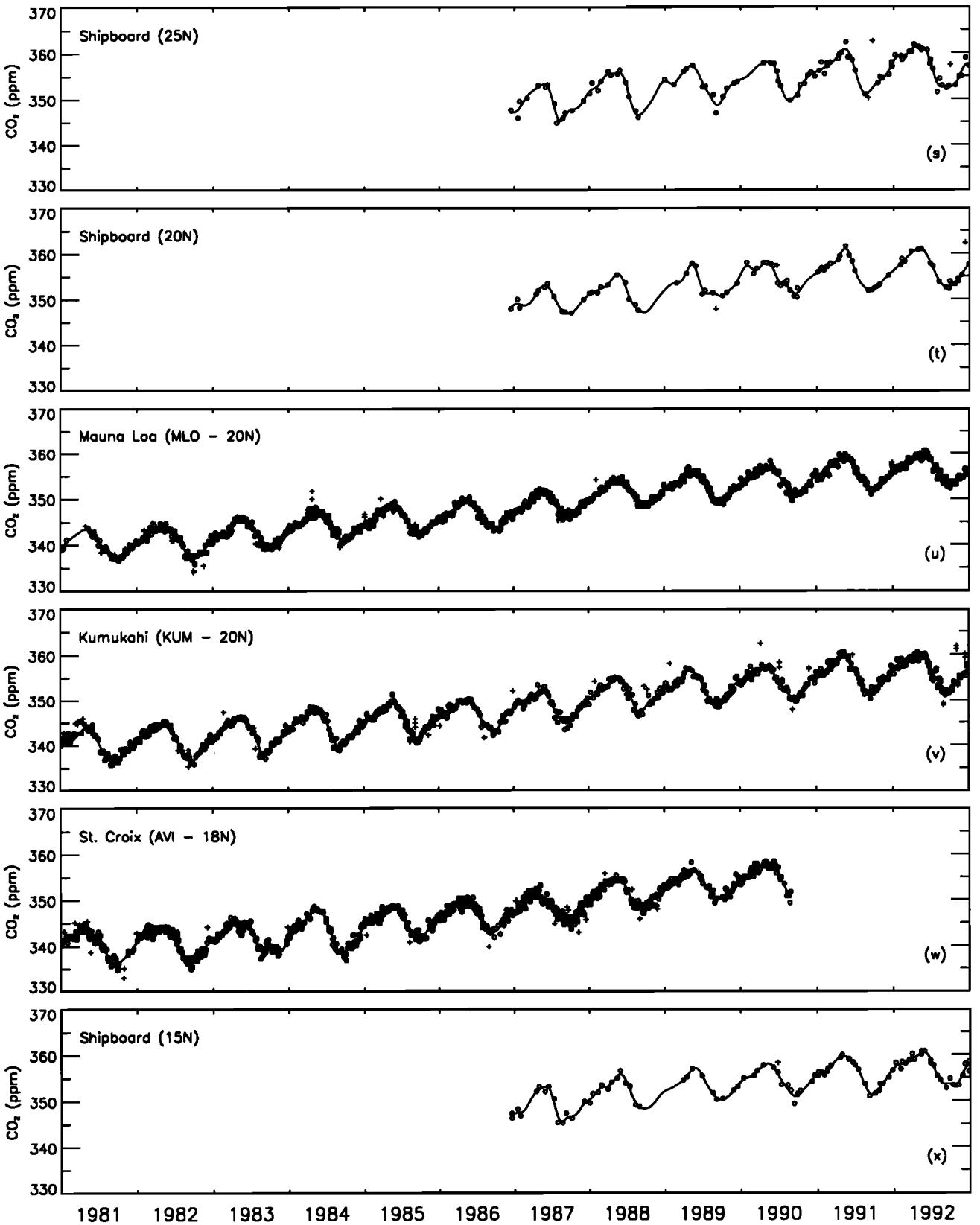

Figure 3. (continued)

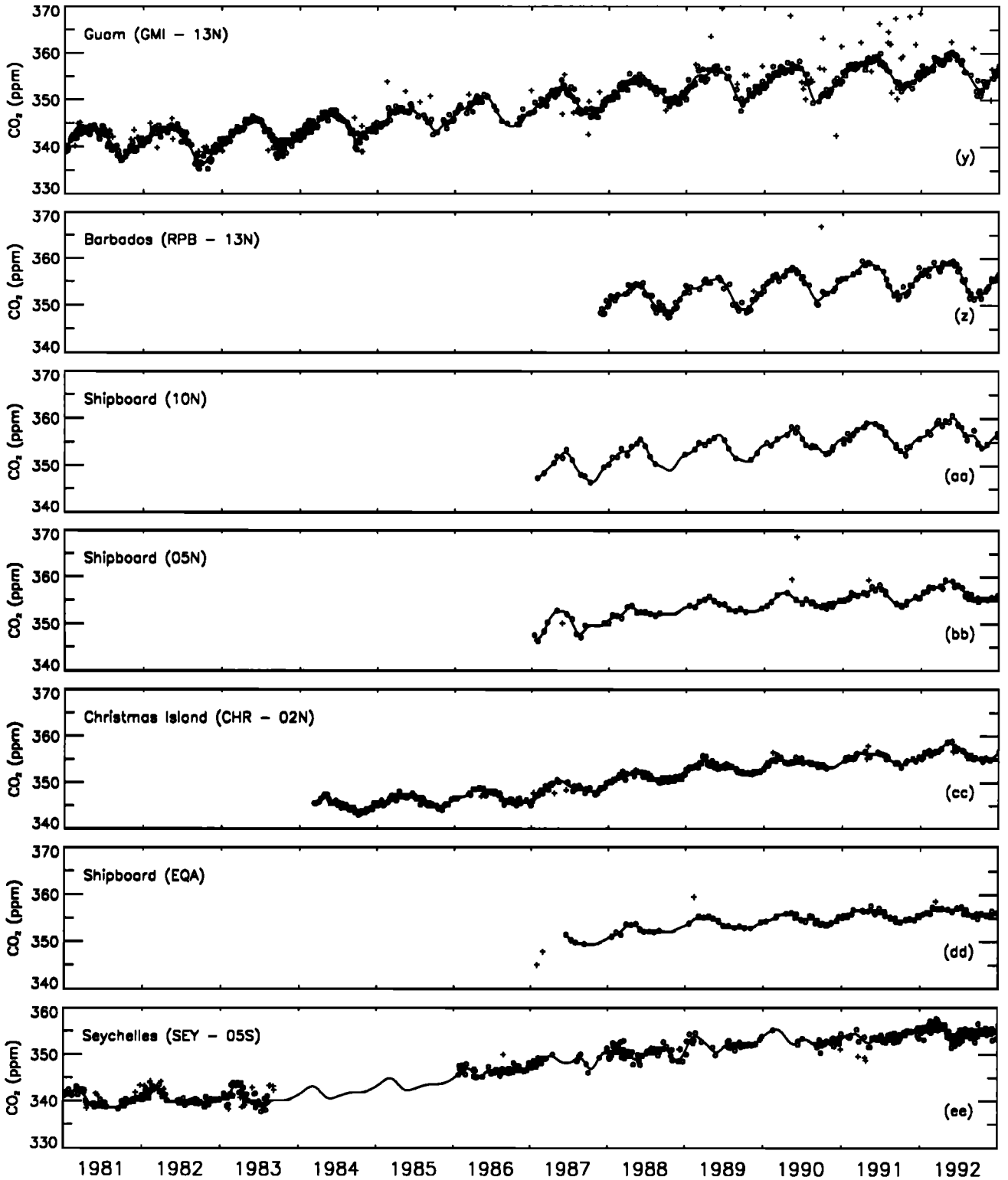

Figure 3. (continued)

since 1989 we have automatically rejected both members of sample pairs when the CO_2 difference between flasks is greater than 0.5 ppm. Previous to 1989, one flask value of a bad pair was sometimes retained, based on the results of curve fitting as described below. Second, the curves shown in Figure 3 that are used for data selection and to calculate monthly and annual means are not the cubic splines used previously but are obtained by the method described in the next section.

Curve Fitting

The curves used for selecting data and calculating monthly and annual means were obtained using a procedure described by *Thoning et al.* [1989]. Briefly, the curves are a combination of a quadratic fit to the trend and a fit of sines and cosines to the annual cycle and its first three harmonics. The residuals from these fits are then digitally filtered with a filter having a full

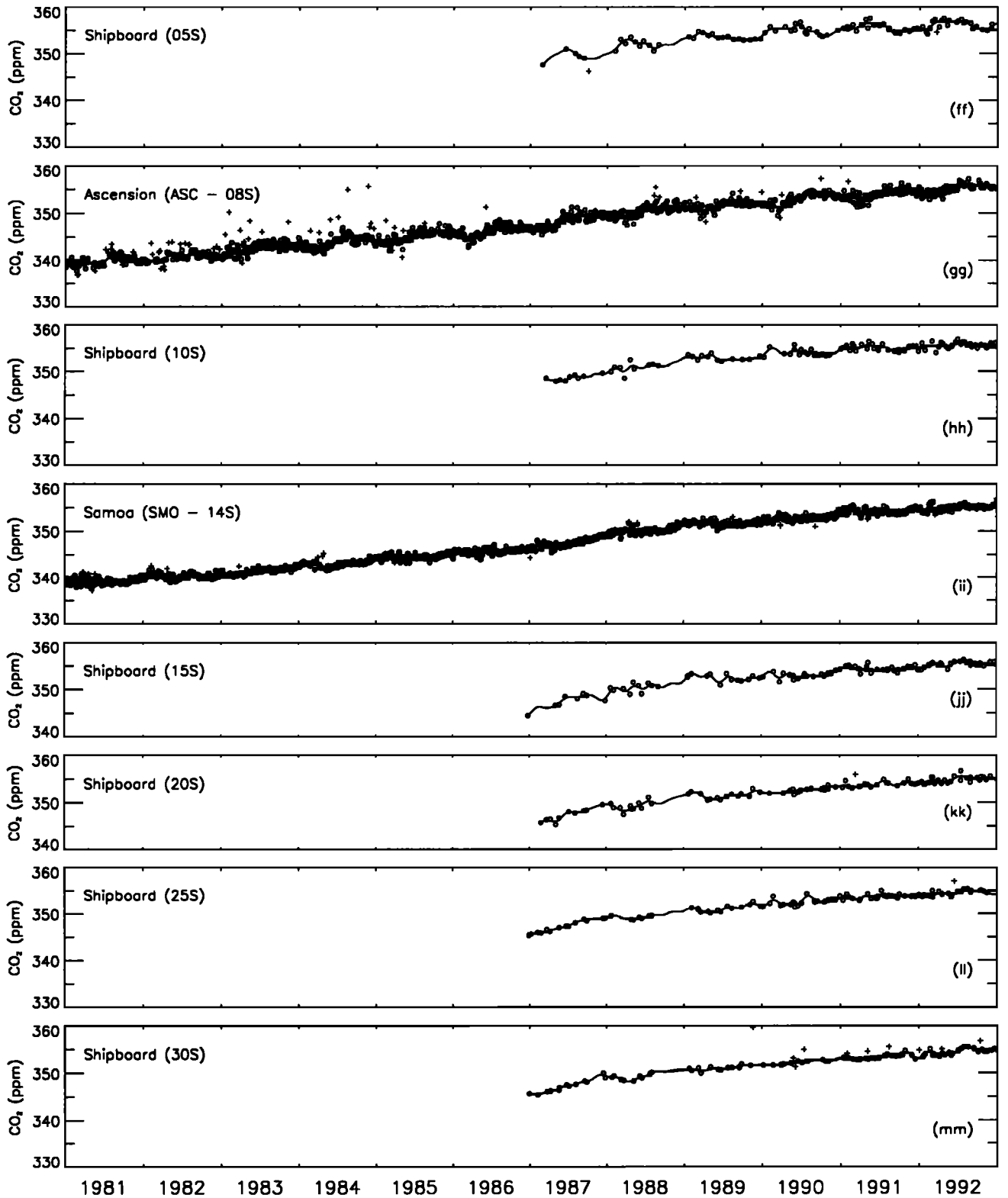

Figure 3. (continued)

width half maximum cutoff at 40 days to remove high-frequency variations. The results of the filtering are then added to the fitted curves. At this point the residual standard deviation of the points from the curve is calculated, and points lying more than $\pm 3\sigma$ from the curve are flagged as not representative of background or regionally well-mixed conditions. The procedure is repeated on the unflagged values until no more points are flagged. The curves obtained by this method follow the deep northern hemisphere summer drawdown better than the previously used cubic spline method (see Figure 3).

A drawback of this objective selection method is that valid samples may be rejected as outliers. An example of this is Station "M" (STM) (Figure 3d), where several samples with high CO_2 are flagged as nonbackground each winter. These

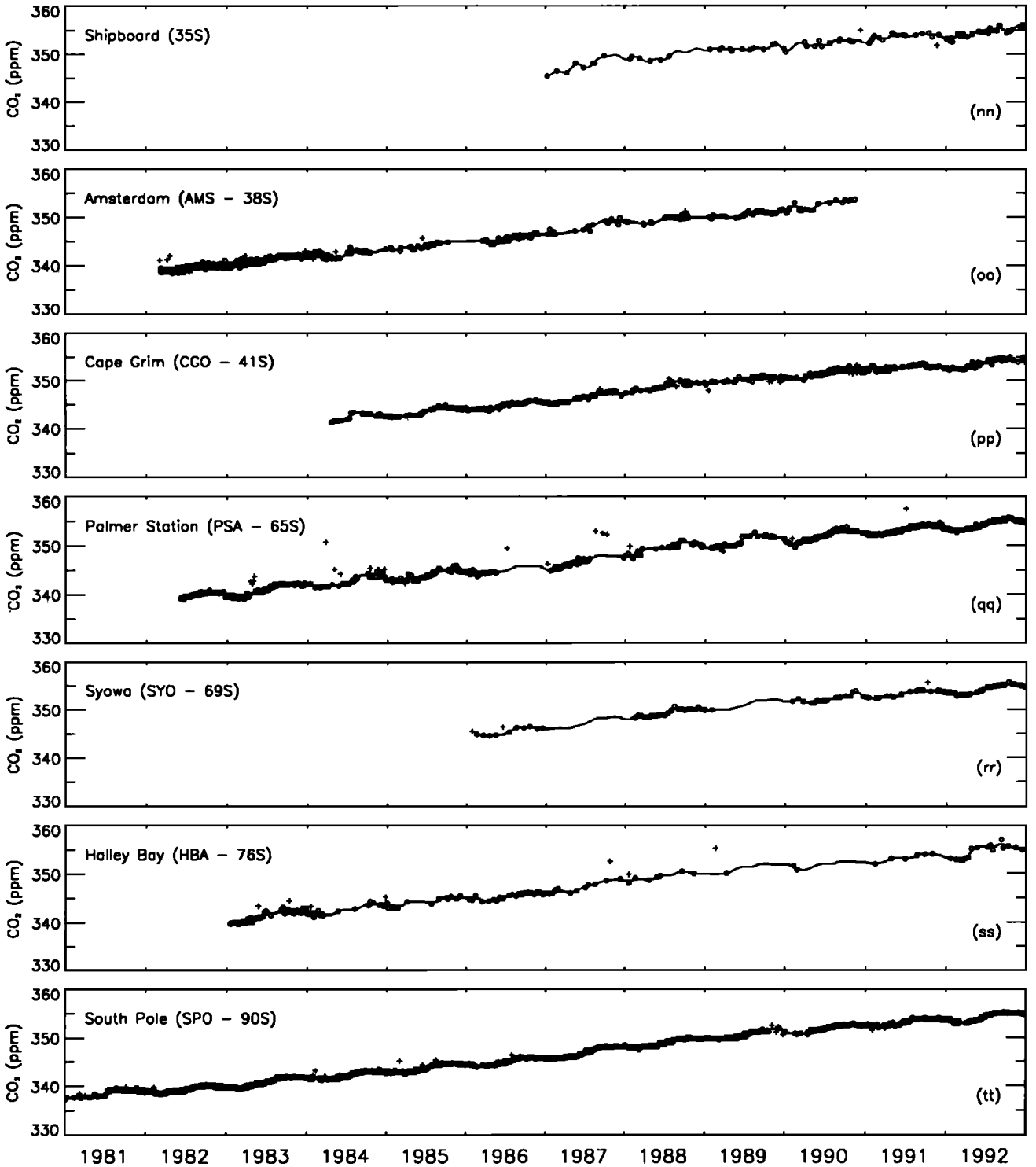

Figure 3. (continued)

samples are associated with transport of polluted air from Europe to the sampling site during winter. We continue to use this method because relatively few samples are flagged as nonbackground, and the resulting biases introduced to the annual means are small. We emphasize that the flagged values are retained in the database, and they may contain useful information.

Smoothed Zonal Representation

Using the curves described above, we can calculate the smoothed, zonally averaged representation of CO_2 mixing ratio, as a function of time and latitude, shown in Figure 4. Starting with January 1, 1981, and proceeding in 2-week time steps, a meridional CO_2 distribution is obtained from the curves fitted to each station time series. A curve of CO_2 versus latitude is fitted to these points at each time step using the method of *Tans et al.* [1989]. A matrix of CO_2 mixing ratios evenly spaced at intervals of 2 weeks and 10° of latitude is then constructed from these curves. This matrix is then plotted using the IDL graphics language [*Research Systems Inc.*, 1991] to arrive at the result shown in Figure 4.

Table 2. Annual Mean CO_2 Mixing Ratio, ppm

Code	Station	1981	1982	1983	1984	1985	1986	1987	1988	1989	1990	1991	1992
ALT	Alert, Canada						348.4	349.7	353.0	355.1	355.5	357.2	357.5
AMS	Amsterdam Island		339.6	341.2	342.5	344.1	345.6	347.9	349.5	350.5	342.5		
ASC	Ascension Island	339.8	340.7	342.7	343.9	345.1	346.2	348.5	350.4	351.6	352.9	353.9	355.1
AVI	St. Croix, Virgin Islands	340.5	340.9	342.0	343.4	345.5	346.8	348.5	351.4	353.5			
AZR	Azores	339.6	341.2	343.0	344.4	346.0	348.8	348.6	351.6			355.8	
BME	Bermuda (east)										355.2	356.1	357.0
BMW	Bermuda (west)										355.1	356.6	356.3
BRW	Barrow, Alaska	341.4	342.7	343.7	345.5	346.8	348.9	349.9	353.4	355.0	356.0	357.6	357.5
CBA	Cold Bay, Alaska	341.2	341.9	343.2	345.6	347.1	348.5	350.1	352.3	354.4	355.3	357.3	357.3
CGO	Cape Grim, Tasmania					343.5	344.8	346.5	348.9	350.3	351.6	352.8	353.5
CHR	Christmas Island					346.0	347.0	348.8	351.3	353.3	354.3	355.4	356.4
CMO	Cape Meares, Oregon			342.9	344.9	347.3	348.2	351.2	352.6	354.4	355.4	356.7	356.3
GMI	Guam, Mariana Islands	341.3	341.0	342.8	344.5	346.1	347.6	349.6	352.1	353.6	354.2	356.1	356.3
HBA	Halley Bay, Antarctica			341.5	342.7	344.3	345.4	347.5					354.7
IZO	Izaña Observatory, Tenerife												356.2
KEY	Key Biscayne, Florida	342.3	341.5	343.5	345.3	346.7	348.1	350.4	352.7	354.4	355.9	356.5	357.3
KUM	Cape Kumukahi, Hawaii	340.4	341.2	342.6	344.3	345.7	346.9	348.8	351.4	352.9	354.3	355.8	356.3
MBC	Mould Bay, Canada	341.8	342.5	343.7	345.6	346.8	348.9	350.1	353.5	355.5	356.0	357.6	357.4
MHT	Mace Head, Ireland												356.1
MID	Sand Island, Midway						347.9	349.9	352.9	354.1	355.2	357.0	356.8
MLO	Mauna Loa, Hawaii	340.4	340.9	342.5	344.2	345.4	346.6	348.7	351.3	352.8	354.1	355.5	356.4
NWR	Niwot Ridge, Colorado	340.1	340.9	342.5	344.6	346.1	346.8	349.1	351.9	353.5	354.7	356.1	356.8
PSA	Palmer Station, Antarctica		339.9	341.0	342.7	344.0		346.9	349.6	350.9	351.9	353.2	354.2
QPC	Qinghai Province, China												356.4
RPB	Ragged Point, Barbados								351.5	352.9	354.7	355.9	355.9
SEY	Seychelles	340.0	340.5				346.4	348.7	350.3	352.2	353.3	353.9	354.8
SHM	Shemya Island, Alaska						349.3	350.4	353.1	354.5	355.0	356.7	357.1
SMO	Matatula Point, Samoa	339.2	340.4	341.4	342.9	344.5	345.7	347.5	350.2	351.7	352.8	354.2	354.9
SPO	South Pole, Antarctica	338.5	339.4	340.8	342.2	343.7	345.0	346.9	349.0	350.6	351.8	353.1	354.1
STM	Station "M"		341.7	342.8	344.7	346.1	347.6	349.1	352.4	354.0	354.8	356.5	356.5
SYO	Syowa, Antarctica						345.5		349.3		352.3	353.3	354.2
TAP	Tae-ahn Peninsula, Korea											359.8	360.6

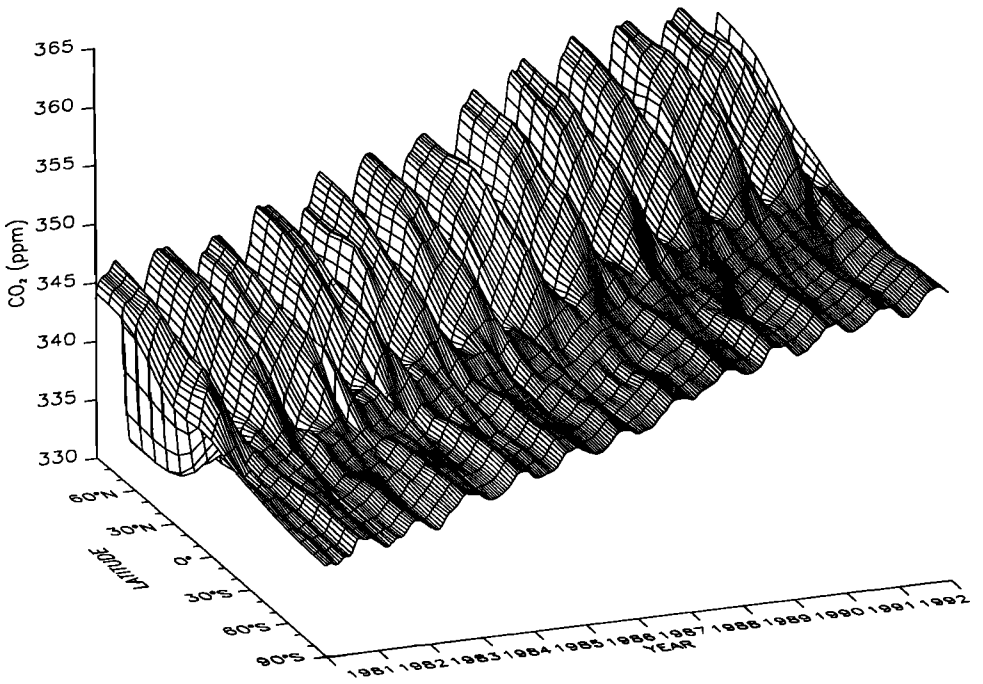

Figure 4. The smoothed, zonally averaged variation with time and latitude of CO_2 mixing ratio for 1981-1992 determined from the CMDL air sampling network.

The smooth CO_2-latitude-time surface is thus a synthesis of more than 17,000 measurements and conveniently highlights many significant features of atmospheric CO_2 variations. The strong seasonality of CO_2 in the northern hemisphere due to photosynthesis and respiration of the terrestrial biosphere is a dominant feature. In this projection (Figure 4) the summer minimum is mostly hidden, but the interannual variability of the seasonality is still apparent. In the southern hemisphere the seasonality is much smaller and the phase is opposite to that in the northern hemisphere. The annual mean CO_2 is higher in the northern hemisphere because anthropogenic emissions occur primarily in this hemisphere. However, during the northern summer, removal of CO_2 from the atmosphere by photosynthesis causes CO_2 to be lower in the northern hemisphere than in the southern. The increasing trend of CO_2 globally is also apparent in Figure 4 and will be discussed quantitatively below. Because several smoothing steps are involved, the patterns apparent in Figure 4 reflect processes occurring over large spatial and long time scales rather than shorter term and more regional effects that may influence the records at each site. For this reason, in the following sections we will use the smoothed representation to extract parameters on global and semihemispheric scales.

Discussion

The 1981-1992 global and semihemispheric annual average CO_2 mixing ratios calculated from the smoothed matrix shown in Figure 4 are presented in Table 3. The estimated uncertainties of the annual means were calculated using a bootstrap analysis that indicates how sensitive a derived parameter is to the distribution of sampling sites used to obtain it. The uncertainties obtained by the bootstrap analysis are probably more realistic than statistics based on the noise or scatter at individual sites, as presented by *Conway et al.* [1988]. In this case we have constructed 100 bootstrap "networks" by choosing 42 sites randomly and with restitution from our actual

Table 3. Semihemispheric and Global Annual Mean CO_2 Mixing Ratios, ppm

Year	30°-90°S	0°-30°S	0°-30°N	30°-90°N	Global
1981	338.79 (0.08)	339.39 (0.13)	340.60 (0.37)	340.65 (0.29)	339.86 (0.14)
1982	339.53 (0.12)	340.31 (0.07)	340.97 (0.06)	341.67 (0.10)	340.62 (0.06)
1983	341.06 (0.09)	341.79 (0.39)	342.62 (0.16)	343.07 (0.12)	342.13 (0.14)
1984	342.47 (0.13)	343.26 (0.29)	344.51 (0.30)	345.06 (0.14)	343.83 (0.16)
1985	343.81 (0.19)	344.71 (0.18)	346.05 (0.29)	346.87 (0.24)	345.36 (0.15)
1986	345.10 (0.18)	345.84 (0.08)	347.23 (0.22)	348.35 (0.19)	346.63 (0.11)
1987	346.86 (0.24)	347.89 (0.13)	349.27 (0.17)	349.97 (0.29)	348.50 (0.11)
1988	349.23 (0.16)	350.18 (0.08)	351.84 (0.10)	352.60 (0.18)	350.96 (0.08)
1989	350.65 (0.12)	351.82 (0.12)	353.47 (0.11)	354.34 (0.16)	352.57 (0.07)
1990	351.83 (0.16)	353.01 (0.14)	354.66 (0.17)	355.28 (0.15)	353.69 (0.08)
1991	353.06 (0.15)	354.15 (0.11)	355.98 (0.07)	356.76 (0.13)	354.99 (0.08)
1992	353.97 (0.19)	355.02 (0.09)	356.59 (0.14)	356.78 (0.16)	355.59 (0.09)

The values in parentheses are 1σ standard deviations determined from the bootstrap analysis.

network and the 14 shipboard latitude bins. In each realization, some sites will be missing and others will be present twice or more often. Only 42 sites are used because Mauna Loa, Hawaii, (MLO), Niwot Ridge, Colorado (NWR), and Izaña Observatory, Tenerife (IZO) are at high altitudes, and TAP is heavily influenced by anthropogenic emissions. The procedure described in the previous section is used to obtain 100 CO_2-latitude-time surfaces similar to the one in Figure 4. Each bootstrap network is required to have either South Pole, Antarctica (SPO) or Palmer Station, Antarctica (PSA), either Matatula Point, Samoa (SMO) or Ascension Island (ASC), and one of Cold Bay, Alaska (CBA), STM, Barrow, Alaska (BRW), and Mould Bay, Canada (MBC) in order to sufficiently constrain the meridional fits. The mean and standard deviation of a given parameter can then be calculated from the 100 bootstrap samples. It is clear from Table 3 that annual means for the marine boundary layer are very well determined from our current network.

Growth Rates

On the basis of the global means in Table 3, CO_2 increased globally at a mean rate of 1.43 ppm yr^{-1} from 1981 to 1992. It is also apparent from Table 3 that there is significant interannual variation of the CO_2 growth rate. Figure 5 shows a plot of biweekly global mean CO_2 mixing ratios calculated from the smoothed values in Figure 4. The solid curve in Figure 5 is the sum of a quadratic fit to the biweekly values and the result of digitally filtering the residuals with a filter having an effective full width half maximum cutoff at 1 year. This curve thus represents the deseasonalized trend with the short-term (less than 1 year) variability removed. The uncertainty of the trend curve is estimated from the bootstrap analysis to have decreased from about 0.15 ppm in the earlier years to 0.08 ppm in more recent years.

The variation of the global CO_2 trend with time is shown in Figure 6 which is the derivative of the solid curve in Figure 5. The largest global growth rate anomalies during the period of these measurements are low growth in 1982 followed by a higher than average increase in 1983, a period of higher than average growth in 1987-1988; and a general decline in the growth rate from the maximum of ~2.5 ppm yr^{-1} in 1987-1988 to ~0.6 ppm yr^{-1} in 1991-1992. Although the bootstrap analysis shows that the growth rate curves are fairly well determined, there is additional uncertainty at the end of 1992 due to end effects associated with the curve-fitting procedure. Because the curves are based on data only through the end of 1992, there is a tendency for the growth rate to turn toward the mean value at the end of the record. The last 6 months of the growth rate curves should therefore be viewed with some caution. A preliminary analysis of available 1993 data suggests that the qualitative features at the end of 1992 in Figures 6 and 7 will not change drastically when the 1993 data are included.

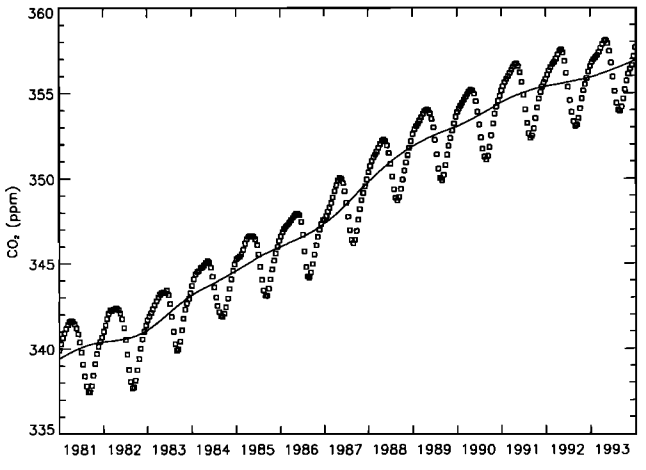

Figure 5. Globally averaged CO_2 mixing ratio variations from 1981 to 1992, at biweekly intervals, calculated from the smoothed representation in Figure 4. The solid curve represents the long-term CO_2 trend, as described in the text.

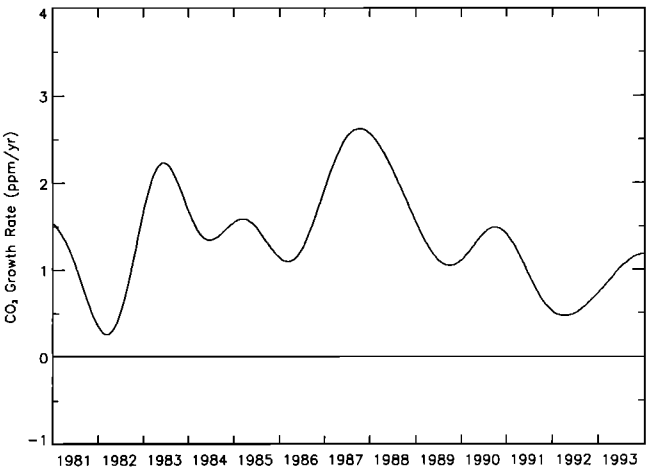

Figure 6. The time variation of the globally averaged CO_2 growth rate. This curve is the derivative of the smooth curve in Figure 5.

Several studies have found a statistical relationship between variations in the CO_2 growth rate and El Niño/Southern Oscillation (ENSO) events [e.g., *Bacastow*, 1976; *Bacastow et al.*, 1980; *Keeling et al.*, 1985; *Thompson et al.*, 1986; *Elliott et al.*, 1991]. The 1982-1983 event received particular attention [*Gaudry et al.*, 1987; *Feely et al.*, 1987; *Fushimi*, 1987]. However, none of these analyses has satisfactorily explained the mechanism by which ENSO affects atmospheric CO_2. *Keeling et al.* [1989b] have used measurements of $^{13}C/^{12}C$ in CO_2 to suggest that the terrestrial biosphere releases more CO_2 to the atmosphere during ENSO events resulting in increased CO_2 growth rates. This explanation is still inconclusive since it is not confirmed by the isotopic measurements of *Francey et al.* [1990]. *Nakazawa et al.* [1993] have used measurements of CO_2 and $^{13}C/^{12}C$ to show that interannual variations in the CO_2 trend from 1984 to 1990 were primarily caused by the terrestrial biosphere. The difficulty in explaining the ENSO connection with the carbon cycle is highlighted by comparing the 1982-1983 and 1986-1987 events. The 1982-1983 ENSO, perhaps the strongest of the century, is associated with an initial decrease in the growth rate followed by a relatively modest rise. The 1986-1987 event was significantly weaker than 1982-1983, but the rise in the CO_2 growth rate was larger, lasted longer, and was not preceded by a marked decrease. Finally, the on again-off again El Niño of 1990-1992 [*Halpert et al.*, 1993] appears to be associated with a period of lower than average CO_2 growth rates. In this case, the climate perturbation caused by the eruption of Mount Pinatubo in 1991 may have interfered with the normal ENSO progression, and the volcano-induced cooling [*Dutton and Christy*, 1992] may be the predominant factor affecting the carbon cycle.

The unusual nature of the low CO_2 growth rate in 1991-1992 is shown in Figure 7 where growth rate curves for the four

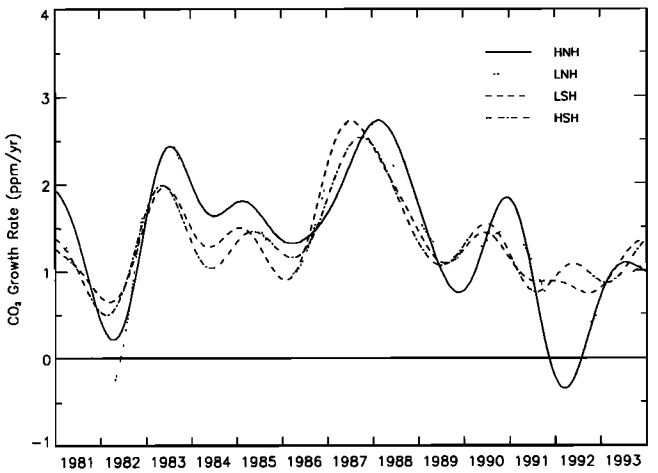

Figure 7. The time variation of the semihemispheric CO_2 growth rate. HNH = 30°-90°N; LNH = 0°-30°N; LSH = 0°-30°S; and HSH = 30°-90°S. Note the very low growth rates in the HNH during 1992.

semihemispheres are plotted. The uncertainty of these curves is estimated from the bootstrap analysis to be ~0.2 ppm yr^{-1} from 1981 to 1987 and ~0.15 ppm yr^{-1} thereafter. From 1981 through 1990 the growth rate variations are fairly coherent and of similar magnitude globally, although there are some differences that may be significant. In 1981-1982 the decline in the CO_2 growth rate occurs earliest in low latitudes of the northern hemisphere. The subsequent increase in the growth rate in 1982 is larger in the northern hemisphere, while a similar but smaller increase occurs in the southern hemisphere. The increasing growth rate in 1986-1987 begins and peaks earliest in the tropical and subtropical latitudes of both hemispheres and later at higher latitudes. In this case the magnitude of the growth rate peak is similar in the four latitude zones but occurs somewhat later at high northern latitudes.

Following a global return to near-average growth rates in 1989-1990, the growth rate declined again globally in 1991. In this case the CO_2 growth rate in the northern hemisphere, especially at high latitudes, is much lower than in the southern hemisphere. In fact, it is apparent from Table 3, that from 30° to 90°N there was no increase in CO_2 during 1992, and the increase from the equator to 30°N was only ~0.6 ppm yr^{-1}. The globally averaged CO_2 increase during 1992 was also ~0.6 ppm, less than half of the average growth rate from 1981 to 1992. The source and sink patterns associated with this dramatic CO_2 growth rate anomaly are discussed in the Two-Dimensional Model Results section.

The spatial and temporal variability of the CO_2 growth rate is shown in more detail in Figure 8. This plot was obtained by calculating CO_2 growth rate curves for deseasonalized slices from the surface of Figure 4, at intervals of 0.05 of sine (latitude) and 14 days. The contour plot was then produced from the growth rate matrix using the IDL routine "CONTOUR" [*Research Systems Inc.*, 1991]. This figure illustrates a slight tendency for CO_2 growth rate perturbations to first appear in the tropical regions of both hemispheres, followed by relatively large anomalies in the middle to high northern latitudes. In 1987-1988, growth rates in excess of 3 ppm yr^{-1} were observed north of 60°N, while during late 1991 and the first half of 1992, the CO_2 growth rate north of 30°N ranged from 0 to -0.5 ppm yr^{-1}.

Latitude Gradients

The measured variation of annual mean CO_2 mixing ratios with latitude is frequently used to evaluate the validity of two- and three-dimensional global carbon budget models [e.g., *Pearman and Hyson*, 1986; *Keeling et al.*, 1989a; *Tans et al.*, 1990]. The latitude gradients determined from the NOAA flask

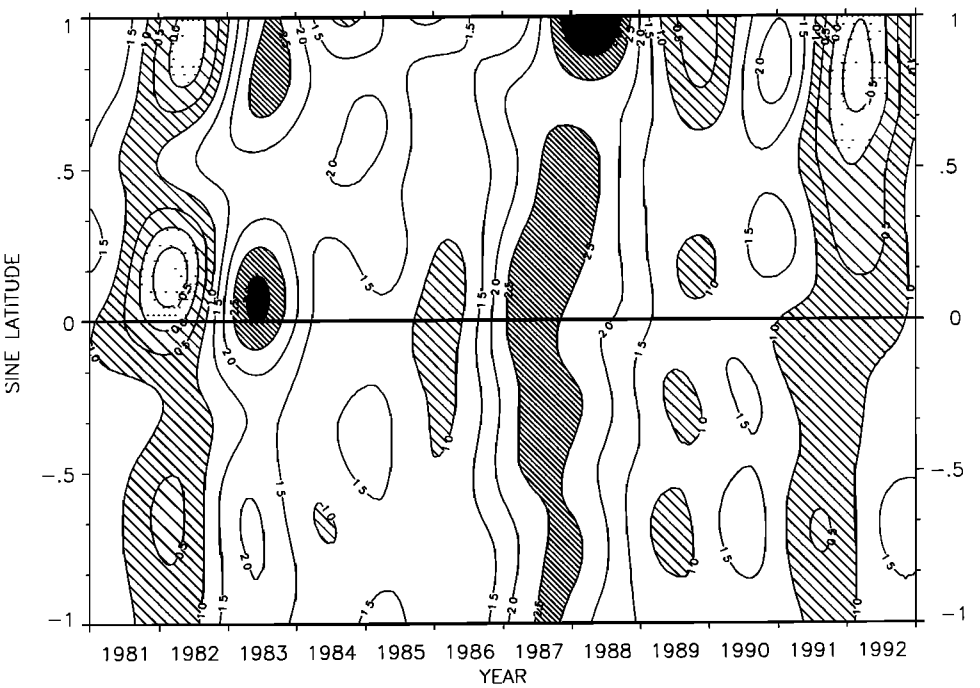

Figure 8. Contour plot of CO_2 growth rate variations with latitude and time. This figure was obtained by differentiating deseasonalized slices from the CO_2 mixing ratio distribution shown in Figure 4.

network data are summarized in Figure 9. Based on examination of the latitude gradients for each year from 1981 to 1992, we show average gradients for 1981-1987, 1988-1991, and the gradient for 1992. For the 1981-1987 and 1988-1991 averages the annual means for each year were normalized to the south pole before calculating the multiyear mean. The error bars in Figure 9 represent ±1 standard error of the mean. For 1992 the error bars represent the standard error of the annual mean obtained by dividing the residual standard deviation from the curve fit by the square root of the number of samples in 1992. The curves in Figure 9 are cubic polynomials fitted to the data by an unweighted least squares method. The curves and the data were then shifted, so the curve is forced to 0 at the south pole. In this way the end points of the curves determine a fairly robust north pole - south pole CO_2 difference. The grouping of years in Figure 9 was chosen to emphasize the observed

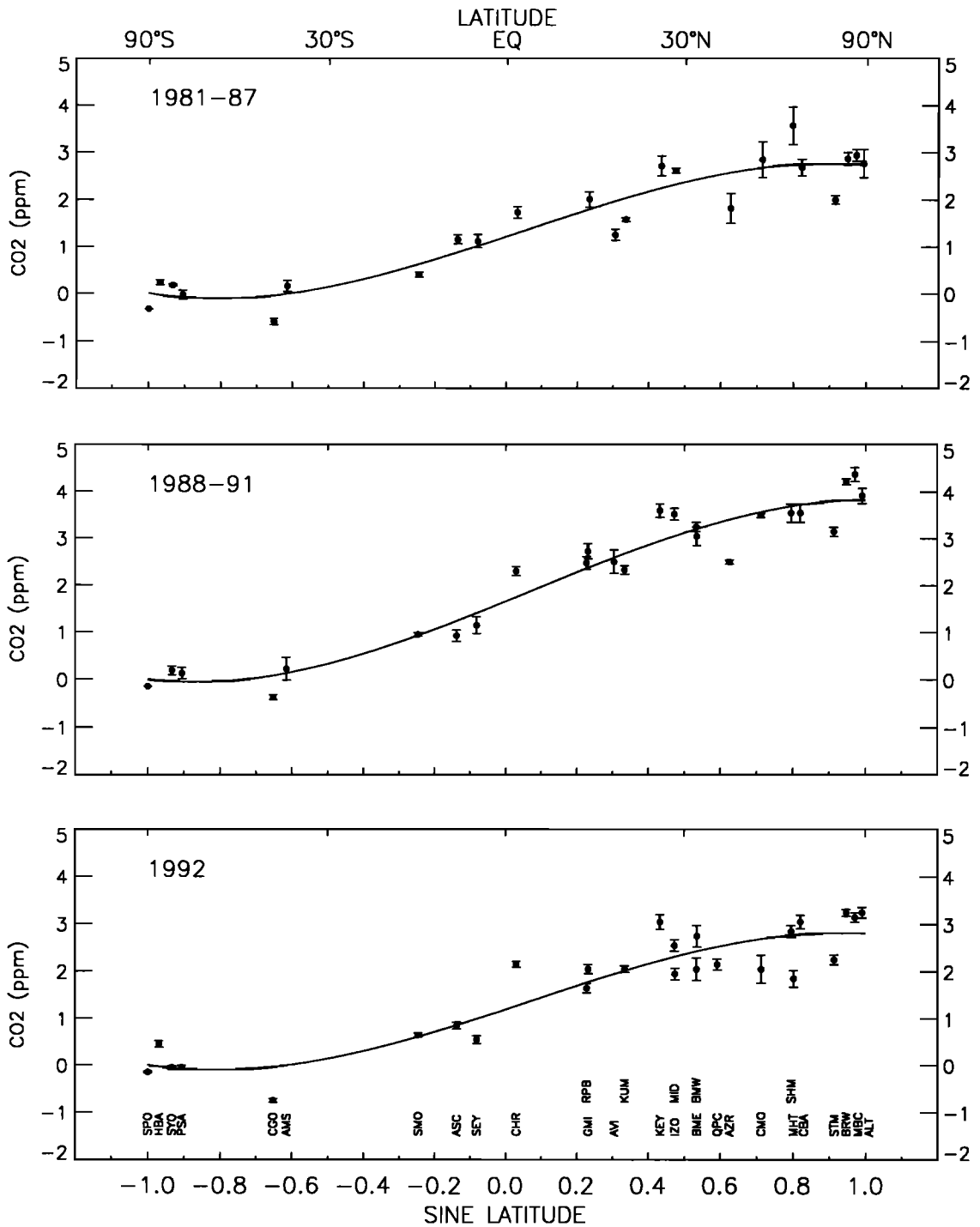

Figure 9. Mean CO_2 latitude gradients for 1981-1987; 1988-1991, and the annual mean gradient for 1992. The curves are cubic polynomials forced to 0 at the south pole. The error bars represent ±1σ standard errors.

variation of the CO_2 latitude gradient. From 1981 to 1987 the north pole-south pole CO_2 difference remained nearly constant at just under 3 ppm. In 1987 the difference shifted to ~4 ppm, a situation that persisted through 1991. In 1992 the difference was again ~3 ppm, similar to the 1981-1987 period.

Cubic polynomials were chosen for the fits in Figure 9 because of their relative stiffness: only the broadest features of the latitude gradients are captured by the curve. There are, however, systematic deviations from this curve that should be noted. At high northern latitudes, ALT, MBC, and BRW tend to lie above the curve, while STM is ~0.5 ppm below it. Christmas Island (CHR), at 2°N, is from 0.5 to 1.0 ppm above the curve. In the southern hemisphere, Cape Grim, Tasmania (CGO) is always below the curve and consistently has the lowest annual mean of our network, slightly lower even than SPO. Finally, the mean CO_2 mixing ratios at the Antarctic coastal sites Halley Bay, Antarctica (HBA), Syowa, Antarctia (SYO), and PSA are generally slightly higher than SPO, which is on the Antarctic plateau.

The mean latitude gradient of CO_2 is primarily due to the emission of CO_2 from fossil fuel combustion, about 90% of which occurs in the northern hemisphere [*Marland and Boden*, 1991]. *Keeling et al.* [1989a] have shown that the latitude gradient has been increasing since the late 1950s as fossil fuel CO_2 emissions have increased. *Tans et al.* [1989] have pointed out that regionally significant CO_2 sources and sinks are needed to maintain the small but persistent spatial gradients evident in Figure 9, given that atmospheric circulation and mixing are constantly working to homogenize the atmosphere. In a later section we present results from a two-dimensional inversion of the data in an attempt to quantify the source and sink patterns responsible for the observations summarized in Figure 9.

Seasonal Variations

The amplitude of the seasonal cycle at each site was calculated for each year by taking the sum of the maximum and minimum differences of the smoothed curve from the long-term trend. The mean seasonal amplitudes for each site for 1981-1992 (or the number of years available) are shown in Figure 10. The error bars in Figure 10 represent ±1 standard deviation. As shown previously [*Conway et al.*, 1988], the seasonal cycle amplitude is highest at high northern latitudes and decreases southward. In the southern hemisphere the amplitude varies from ~1 to 2 ppm.

Two sites worth special note in Figure 10 are SHM and TAP. These sites were chosen based on three-dimensional model results for CO_2 and CH_4, respectively [*Fung et al.*, 1983, 1991], which showed strong seasonal CO_2 variations over continental interiors and a large CH_4 source in Asia. SHM, CBA, and Mace Head, Ireland (MHT) are at nearly the same latitude, but SHM is downwind from and relatively close to the Asian continent. The measured average seasonal CO_2 amplitude at SHM is ~19 ppm, the highest in our network, and even higher than predicted by *Fung et al.* [1983] for this location. The site at TAP was chosen primarily to sample the large Asian source of CH_4, but *Fung et al.* [1983] also show large CO_2 seasonal amplitudes for this region. With only 2 years of data we have observed amplitudes of ~12 and 22 ppm, consistent with the predicted magnitude and the strong gradients of the seasonal amplitude in continental coastal regions.

Several previous studies have looked for trends in the CO_2 seasonal amplitude as an indication of possible CO_2 fertilization of the terrestrial biosphere [*Cleveland et al.*, 1983; *Bacastow et al.*, 1985; *Enting*, 1987; *Thoning et al.*, 1989; *Manning*, 1993].

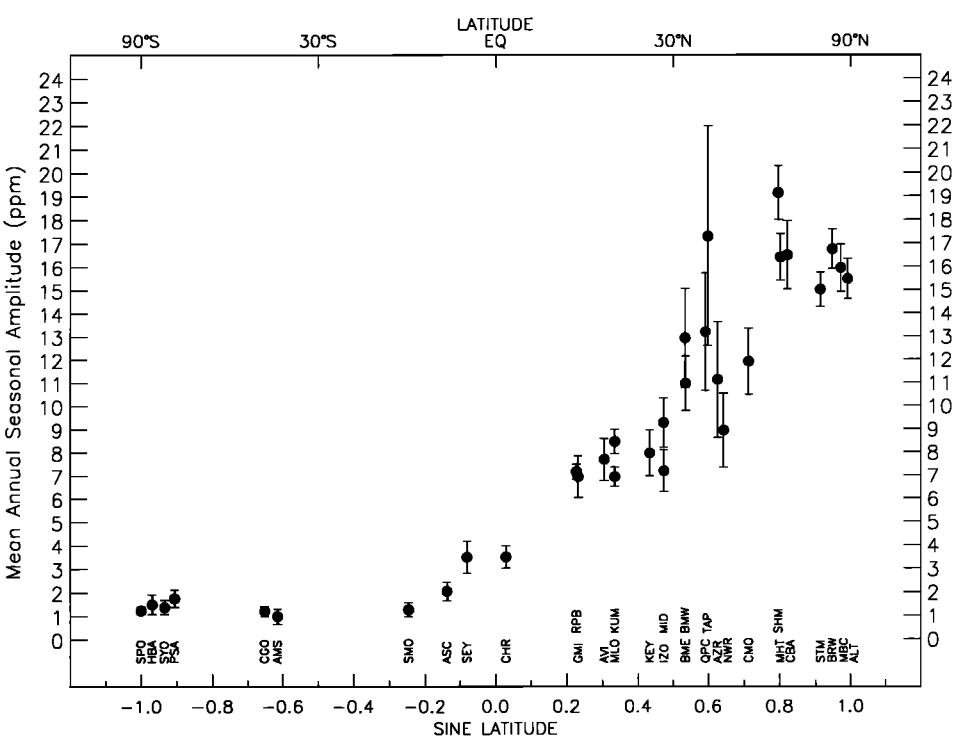

Figure 10. The mean peak-to-peak amplitudes of the seasonal cycle for the flask network sites. The error bars represent ±1 standard deviation.

An examination of the variation with time of the peak-to-peak seasonal amplitude for the flask network data showed no significant trend in amplitude. However, as pointed out previously [*Conway et al.*, 1988], it is difficult to determine changes in the amplitude from relatively sparse sampling and large natural variability. As an alternative approach, we computed the CO_2 annual growth rate for each month of the year for all flask sampling sites. The results for MBC are shown as an example in Figure 11, where the growth rate for each month was determined by linear regression of the monthly means, the error bars represent the one sigma uncertainty of the slope [*Bevington*, 1969], and the horizontal line represents the average growth rate for the period of record. For MBC there is a tendency for lower growth rates in June, July, and August and higher growth rates in December, January, and February. This difference in growth rates suggests that the amplitude of the seasonal cycle at MBC is indeed increasing at the rate of ~0.3 ppm yr^{-1}. This pattern is observed at several northern hemisphere sites (ALT, BRW, STM, CBA), but the result is barely significant, and it is not observed at all sites. We have performed this calculation for semihemispheric averages of the smoothed representation of Figure 4 and found no significant summer-winter growth rate difference. We conclude therefore that based on flask data alone, there has been no significant trend in the amplitude of the seasonal cycle during 1981-1992.

Two-Dimensional Model Results

The CO_2 distribution and variations measured at the CMDL network sites are the combined result of CO_2 sources and sinks and atmospheric transport. Thus the extraction of source and sink information from the CO_2 measurements requires an atmospheric transport model. In this section we present results obtained using the two-dimensional model described in detail by *Tans et al.* [1989] to deduce source and sink patterns from the measurements. Briefly, the model uses the two-dimensional (latitude, altitude) advective-diffusive transport fields derived by *Plumb and Mahlman* [1987] from a three-dimensional general circulation model [*Mahlman and Moxim*, 1978]. The CO_2 distribution at the surface is specified at biweekly intervals by the meridional fits to the smoothed site data (the same meridional curves used to generate Figure 4). At each time step, CO_2 is redistributed by the model transport, and the new surface CO_2 distribution is adjusted to agree with the measurements by inserting surface sources and sinks as needed. In other words, the model calculates the sources and sinks needed to maintain the observed small spatial atmospheric CO_2 gradients that persist against the tendency of atmospheric circulation to smooth them out. An advantage of this approach is that the latitudinal distribution of sources and sinks is derived from the observations with no a priori assumptions about carbon budgets. The disadvantage of the two-dimensional model is that longitudinal variations are not represented. Most of our network sites are in the marine boundary layer, whereas strong sources and sinks exist on the continents. This mismatch leads to some misallocation of sources as a function of latitude by the two-dimensional model [*Tans et al.*, 1989]. Also, this approach gives no information concerning the processes responsible for the derived sources and sinks.

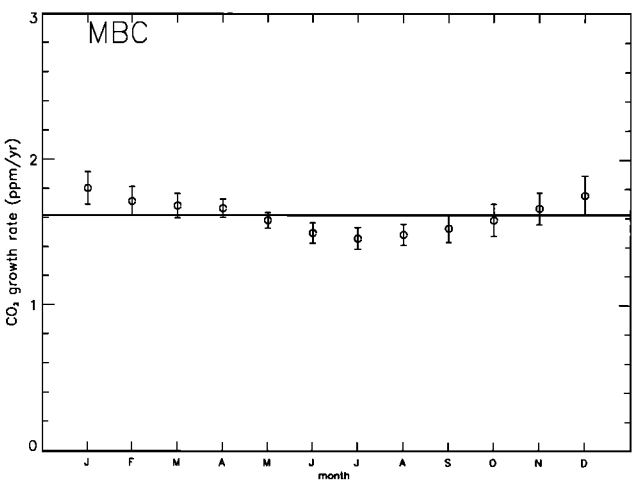

Figure 11. The variation of the CO_2 growth rate by month at MBC. Each symbol represents the trend determined by a linear regression fit to monthly means for each month for 1981-1992. The error bars represent the 1σ standard deviation of the slopes.

The annual mean sources and sinks calculated by the two-dimensional model are given in Table 4, where the uncertainties are 1σ standard deviations obtained by the bootstrap method described above. The CO_2 emissions from fossil fuel combustion through 1989 are from *Marland and Boden* [1991]; the 1990-1991 values are estimates based on preliminary data (T. Boden, personal communication, 1993), and for 1992 we use the 1991 estimate. The global atmospheric increase given in Table 4 is the difference between the fossil fuel emissions and the total global sink. It is important to note that the calculated global atmospheric increase results directly from the measurements, and the total global sink follows directly from the measurements and the estimated fossil fuel emissions. These results are therefore model independent. The latitudinal distribution of sources and sinks is model dependent, and although the model is run with 20 equal area latitude bands, we present the results on a coarser scale (four bands) to avoid over-interpreting possible model dependent features.

The annual average global atmospheric CO_2 increase for 1981-1992 is plotted in Figure 12 together with the annual fossil fuel emissions. The interannual variability of the atmospheric increase is large relative to fossil fuel emissions, ranging from ~20 to 80% of the fossil fuel total. However, these variations are small relative to the total exchanges of CO_2 between the atmosphere and the oceans (~100 Gt C yr^{-1}) and the atmosphere and the terrestrial biosphere (~60 Gt C yr^{-1}) [*Bolin et al.*, 1977]. The largest year-to-year changes in the atmospheric increase occurred in 1982-1983 and 1986-1987 in association with El Niño/Southern Oscillation events and are of the order of 2-3 Gt C yr^{-1}. The total amount of carbon burned in the oil well fires during the Persian Gulf war has been estimated to be 0.1 - 0.2 Gt C [*Hobbs and Radke*, 1992], which is too small to be detected among the natural variations of the carbon cycle. Since 1988, there has been a general decrease in the atmospheric growth rate. Because the fossil fuel CO_2 emissions have increased or remained nearly level, an increasing natural CO_2 sink is needed to account for the observations.

The annual average sources and sinks for the four semihemispheres (Table 4) are plotted in Figure 13. The latitude band from 30° to 90°N (high northern hemisphere (HNH)) is a sink of 2 to 5 Gt C yr^{-1}. The tropics and subtropics of the northern hemisphere (lower northern hemisphere (LNH)) are a source of CO_2 to the atmosphere ranging from 0 to ~2 Gt C yr^{-1}, with significant interannual variability. The southern tropic and subtropic zone (LSH) is a smaller source of ~0 to 1 Gt C

Table 4. Annual Mean CO_2 Sources and Sinks, Gt C yr^{-1}

Year	30°-90°S	0°-30°S	0°-30°N	30°-90°N	Global	Fossil	Atmospheric Increase
1981	-0.15 (0.17)	-0.75 (0.47)	2.80 (1.05)	-4.51 (0.64)	-2.61 (0.21)	5.13	2.52 (0.21)
1982	-1.07 (0.25)	0.71 (0.33)	0.25 (0.20)	-3.65 (0.27)	-3.76 (0.53)	5.09	1.33 (0.53)
1983	0.15 (0.46)	1.07 (1.23)	0.35 (0.83)	-2.48 (0.24)	-0.91 (0.34)	5.09	4.17 (0.34)
1984	-0.46 (0.40)	0.52 (0.76)	0.81 (0.81)	-2.71 (0.39)	-1.84 (0.25)	5.24	3.40 (0.25)
1985	-0.79 (0.46)	0.47 (0.60)	0.31 (0.75)	-2.25 (0.48)	-2.26 (0.18)	5.37	3.11 (0.18)
1986	-0.74 (0.36)	-0.05 (0.55)	-0.01 (0.60)	-2.30 (0.39)	-3.10 (0.37)	5.55	2.45 (0.37)
1987	-0.40 (0.68)	1.11 (0.77)	0.94 (0.90)	-2.32 (0.90)	-0.67 (0.18)	5.66	4.99 (0.18)
1988	-0.51 (0.26)	0.33 (0.36)	1.52 (0.47)	-2.37 (0.27)	-1.03 (0.23)	5.90	4.87 (0.23)
1989	-1.55 (0.31)	0.39 (0.47)	1.00 (0.50)	-2.92 (0.25)	-3.08 (0.19)	6.02	2.93 (0.19)
1990	-1.38 (0.42)	0.50 (0.57)	0.92 (0.50)	-3.48 (0.36)	-3.43 (0.10)	6.15	2.71 (0.10)
1991	-1.67 (0.45)	-0.17 (0.37)	1.51 (0.32)	-3.85 (0.29)	-4.18 (0.14)	6.10	1.91 (0.14)
1992	-1.50 (0.46)	-0.10 (0.34)	1.87 (0.58)	-4.98 (0.37)	-4.71 (0.11)	6.10	1.39 (0.11)

The values in parentheses are 1σ standard deviations determined from the bootstrap analysis.

yr^{-1}. The zone from 30° to 90°S (HSH) tends to be a CO_2 sink that appears to have increased from ~0.5 Gt C yr^{-1} during 1981-1988 to almost 2 Gt C yr^{-1} from 1989 to 1992.

Examination of Figure 13 reveals contrasts among the 1982/1983, 1986/1987, and 1992 CO_2 growth rate anomalies. In 1982 a relatively large HNH sink, a small LNH source, and a large HSH sink combined to produce a low CO_2 increase. In 1986 the low atmospheric increase results mainly from near-zero CO_2 sources in the northern and southern tropics and subtropics. The high global growth rate in 1983 results from a decrease in the HNH sink, an increase in the LSH source, and the absence of a southern hemisphere ocean sink. The CO_2 rebound in 1987 is almost entirely due to the reappearance of the northern and southern tropical and subtropical sources. The decrease in the CO_2 growth rate since 1988 results mainly from an increasing sink in the northern middle and high latitudes. The drastic decline in 1992 is due to an increase in this sink from 3.9 Gt C yr^{-1} in 1991 to 5.0 Gt C yr^{-1} in 1992.

It is interesting to compare the source and sink patterns of Figure 13 to the CO_2 growth rate variations in Figure 8. In general, the source and sink patterns are consistent with the CO_2 growth rate variations (as they should be, since they are derived from the same data). However, one notable feature in the higher-resolution growth rate plot is lost in the coarser source and sink plots. In 1987-1988 a period of extremely high growth rates is observed in the Arctic. These high growth rates are clearly supported by the data from the Arctic sites. The 20 latitude band two-dimensional model accounts for the period of high CO_2 growth with a 0.8 Gt C yr^{-1} source in the highest northern latitude zone (>64°N). The existence of this sudden high-latitude CO_2 source is unlikely, and we believe this result could be due to a lack of high-latitude continental sampling sites in our network. If such sites were included, we believe that the CO_2 source would probably appear at lower latitudes. By grouping the source and sink results into only four latitude zones, we have tried to obtain a robust result that still reveals important aspects of the CO_2 source and sink distribution.

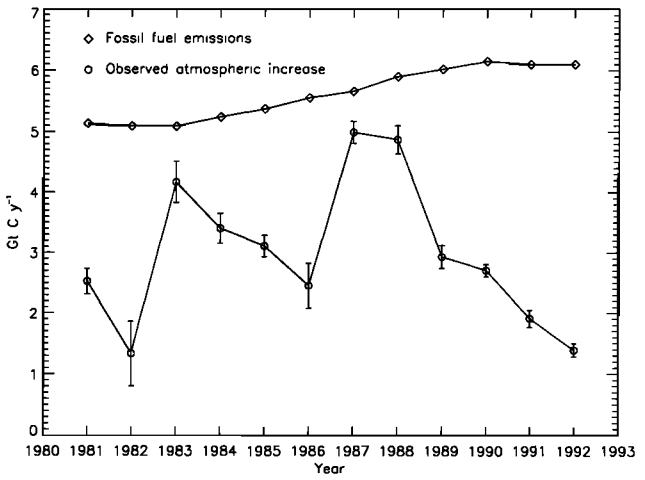

Figure 12. The circles represent the annual average global atmospheric CO_2 increase for 1981-1992 in gigaton (Gt) of carbon, determined from flask network data. The error bars are 1σ standard deviations calculated by a bootstrap analysis. The annual average fossil fuel CO_2 emissions are shown for comparison. The 1990-1992 fossil fuel values are estimates.

The variations of sources and sinks in Figure 13 also suggest an explanation for the variations in the annual mean CO_2 latitude gradient (Figure 9). The increase in the latitude gradient in 1988 is associated with an increase in the LNH source in that year. Then in 1989 the HSH sink increased from 0.5 to 1.6 Gt C yr^{-1}, which combined with a relatively high LNH source continued to offset the increasing HNH sink through 1991. The increase in the HNH sink in 1992 also accounts for the latitude gradient returning to its previous value of ~3 ppm.

The interpretation of the time series of CO_2 sources and sinks derived from atmospheric CO_2 measurements requires consideration of the fact that the network is continually evolving. A few sites have been dropped from the network and several have been added. The biggest change occurred in 1987 when we began shipboard sampling in the Pacific. It is possible that the addition of sites could bias the source and sink time series obtained from the two-dimensional model.

The effect of the network expansion is partly contained in the uncertainties derived from the bootstrap analysis. For example, if the addition of ALT to the network in 1985 caused a sudden change in the source and sink pattern in that latitude band, it would appear in some of the bootstrap runs but not in others, and this would increase the standard deviations of the calculated annual mean sources and sinks. As seen in Table 4, the bootstrap uncertainties are relatively low, suggesting that adding sites has not severely biased the results. The benefit of adding sites is that the uncertainties have decreased as the network has

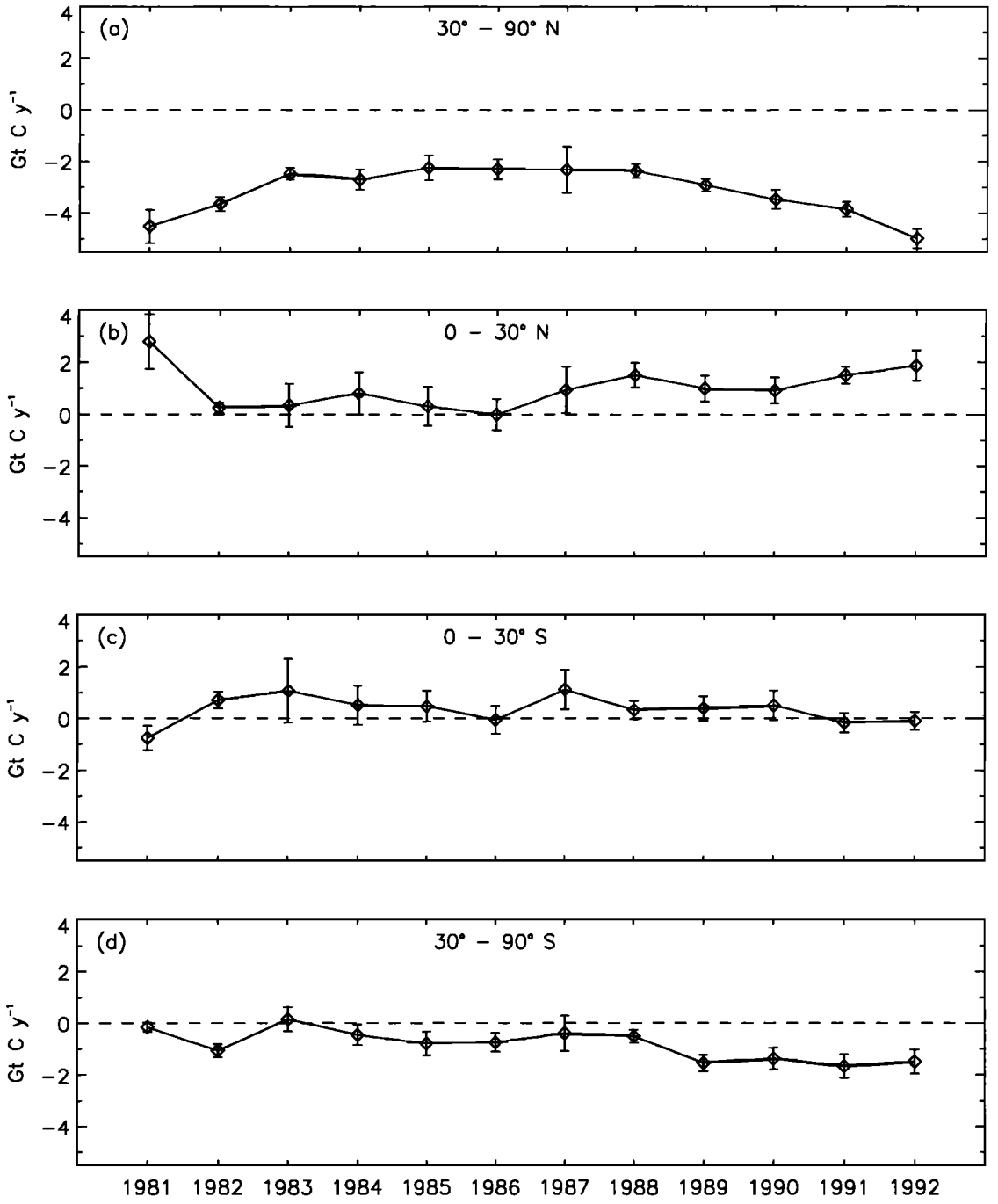

Figure 13. Annual mean CO_2 sources calculated from a two-dimensional model and the CMDL flask network data for the four semihemispheres: (a) 30°-90°N; (b) 0°-30°N; (c) 0°-30°S; and (d) 30°-90°S. The symbols represent the sources calculated by the two-dimensional model, and the error bars represent ±1 standard deviation calculated from the bootstrap analysis.

grown. We have also investigated the bias question by running the two-dimensional model without the shipboard data. While some differences are seen in the latitude bands covered by the ships, the semihemispheric annual mean sources are very similar to those presented in Table 4.

One reason that little or no bias has been introduced is that until very recently, new sites have been chosen according to the same criteria used to construct the original network: remote, marine boundary layer locations, sampling well-mixed air representative of large time, and space scales. Addition to the network of continental sites and sites closer to source regions (e.g., QPC and TAP) will probably introduce more serious biases. In fact, TAP was omitted from the two-dimensional model runs presented here for precisely that reason. While these kinds of sites are needed to better determine the global carbon budget, we will need innovative techniques to assimilate the data into our existing time series.

Although the two-dimensional model offers no information on the processes responsible for the observed source and sink variations, it is interesting to speculate on some possibilities.

Our fossil fuel emission estimate for 1992 simply assumes the same emissions as in 1991. It has been suggested that the economic disruption associated with the collapse of the former Soviet Union (FSU) may have resulted in a decrease of up to 30% in CO_2 emissions from the FSU [*Brown et al.*, 1992]. Applying this to the 1989 emission data of *Marland and Boden* [1991] gives a decline of ~0.3 Gt C yr^{-1}. If a decline in emissions this large is in fact supported by the fossil fuel production data, and if it is not offset by increases elsewhere, e.g., China, it would be a significant contribution to the 1992 growth rate decline. However, using level emissions from 1991 to 1992, the two-dimensional model shows a change in the northern hemisphere sink of 1.1 Gt C yr^{-1}, more than 3 times the possible FSU decline. Thus while a decrease in CH_4 emissions from the FSU has been suggested as an explanation for the dramatic decrease in the CH_4 growth rate in 1992 [*Dlugokencky et al.*, 1994], it appears that the recent decline of the CO_2 growth rate cannot be similarly explained.

Another explanation postulated for the increased northern hemisphere CO_2 sink is an increased flux of CO_2 into the oceans due to cooling of the oceans resulting from the global cooling following the eruption of Mount Pinatubo. This explanation is not supported by $^{13}C/^{12}C$ measurements of CO_2 from samples collected at the CMDL network (P. Ciais et al., unpublished data, 1994). Those results indicate that a large fraction of the northern hemisphere sink in 1992 was in the terrestrial biosphere. Sea surface temperature data available from the National Meteorological Center [*Reynolds and Marsico*, 1993] indicate that the global sea surface has cooled by about 0.15 K since the Pinatubo eruption. If we assume that the average thickness of the surface layer is 70 m, about 0.4 Gt C could have entered the surface ocean in 1 year due to the cooling.

Thus although the evidence to date points to the terrestrial biosphere as the likely cause for the 1992 CO_2 growth rate anomaly, the mechanism of the effect is still not established. Two possibilities are increased carbon storage by photosynthesis or a decrease in respiration. A decrease in respiration is consistent with the Pinatubo cooling, since respiration depends strongly on temperature [*Townsend et al.*, 1992]. In any case, since it is unlikely that the natural carbon cycle has shifted to an entirely new mode, the decreased CO_2 growth rate in 1992 probably reflects a temporary perturbation, and we expect a return to higher CO_2 growth rates.

Conclusions

The spatial and temporal variations of atmospheric CO_2 have been determined by measurements of samples collected at a geographically extensive network of sites from 1981 through 1992. The observed variations cannot be accounted for by variations in fossil fuel emissions. We have used a two-dimensional transport model to calculate CO_2 sources and sinks from the measured atmospheric distribution.

We find that the decline in the CO_2 growth rate since 1988 is mainly due to an increase in the northern hemisphere CO_2 sink. The very low CO_2 increase in 1992 is due to an increase of this sink from 3.9 Gt C yr^{-1} in 1991 to 5.0 Gt C yr^{-1} in 1992. The increase in the annual mean north-south CO_2 gradient is mostly due to an increase of the southern ocean sink from ~0.5 Gt C yr^{-1} in 1981-1987 to ~1.5 Gt C yr^{-1} in 1988-1992. The data suggest that the amplitude of the CO_2 seasonal cycle is increasing in the Arctic, but longer records will be needed to establish the significance of this result.

Because our current network inadequately measures the zonal inhomogeneity of the atmospheric CO_2 distribution, we have used our two-dimensional model results to infer source and sink variations only on broad time and space scales. Inclusion of carefully selected sites in continental interiors will address this limitation. A three-dimensional analysis and more extensive $^{13}C/^{12}C$ measurements are needed to make the important distinction between terrestrial and marine sources and sinks.

Acknowledgments. We thank the agencies listed in Table 1 and the Blue Star Line for their support and assistance in our flask sampling program. Support for CMDL activities at the South Pole Station is provided by the National Science Foundation. We also thank the many individuals who have collected the samples on which this work is based. Their conscientious efforts, in frequently extreme environments, are essential to the success of this project. Partial support for this work has been provided by the Atmosphere-Ocean Carbon Exchange, and Atmospheric Chemistry Projects of NOAA's Climate and Global Change Program, and also by the Environmental Protection Agency.

References

Bacastow, R. B., Modulation of atmospheric carbon dioxide by the Southern Oscillation, *Nature, 261*, 116-118, 1976.

Bacastow, R. B., J. A. Adams, C. D. Keeling, D. J. Moss, and T. P. Whorf, Atmospheric carbon dioxide, the Southern Oscillation, and the weak 1975 El Niño, *Science, 210*, 66-68, 1980.

Bacastow, R. B., C. D. Keeling, and T. P. Whorf, Seasonal amplitude increase in atmospheric CO_2 concentration at Mauna Loa, Hawaii, 1959-1982, *J. Geophys. Res., 90*, 10529-10540, 1985.

Bevington, P. R., *Data Reduction and Error Analysis for the Physical Sciences*, 336 pp., McGraw-Hill, New York, 1969.

Bolin, B., E. T. Degens, P. Duvigneaud, and S. Kempe, The global biogeochemical carbon cycle, in *SCOPE 13-The Global Carbon Cycle*, edited by B. Bolin, E. T. Degens, S. Kempe, and P. Ketner, 491 pp., John Wiley, New York, 1977.

Brown, L. R., C. Flavin, and H. Kane, Vital signs, in *The Trends That are Shaping our Future*, 131 pp., Norton-Holland, New York, 1992.

Cleveland, W. S., A. E. Freeny, and T. E. Graedel, The seasonal component of atmospheric CO_2: Information from new approaches to the decomposition of seasonal time series, *J. Geophys. Res., 88*, 10,934-10,946, 1983.

Conway, T. J., P. Tans, L. S. Waterman, K. W. Thoning, K. A. Masarie, and R. H. Gammon, Atmospheric carbon dioxide measurements in the remote global troposphere, 1981-1984, *Tellus, 40*(B), 81-115, 1988.

Dlugokencky, E. J., K. A. Masarie, P. M. Lang, P. P. Tans, L. P. Steele, and E. G. Nisbet, A dramatic decrease in the growth rate of atmospheric methane in the northern hemisphere during 1992, *Geophys. Res. Lett., 21*, 45-48, 1994.

Dutton, E. G., and J. R. Christy, Solar radiative forcing at selected locations and evidence for global lower tropospheric cooling following the eruptions of El Chichón and Pinatubo, *Geophys. Res. Lett., 19*, 2313-2316, 1992.

Elkins, J. W., T. M. Thompson, T. H. Swanson, J. H. Butler, B. D. Hall, S. O. Cummings, D. A. Fisher, and A. G. Raffo, Decrease in the growth rates of atmospheric chlorofluorocarbons 11 and 12, *Nature, 364*, 780-783, 1993.

Elliott, W. P., J. K. Angell, and K. W. Thoning, Relation of atmospheric CO_2 to tropical sea and air temperatures and precipitation, *Tellus, 43*(B), 144-155, 1991.

Enting, I. G., The interannual variation in the seasonal cycle of carbon dioxide concentration at Mauna Loa, *J. Geophys. Res., 92*, 5497-5504, 1987.

Enting, I. G., and J. V. Mansbridge, Seasonal sources and sinks of atmospheric CO_2: Direct inversion of filtered data, *Tellus, 41*(B), 111-126, 1989.

Enting, I. G., and J. V. Mansbridge, Latitudinal distribution of sources and sinks of CO_2: Results of an inversion study, *Tellus, 43*(B), 156-170, 1991.

Feely, R. A., R. H. Gammon, B. A. Taft, P. E. Pullen, L. S. Waterman, T. J. Conway, J. E. Gendron, and D. P. Wisegarver, Distribution of chemical tracers in the eastern equatorial Pacific during and after the 1982-1983 El Niño/Southern Oscillation event, *J. Geophys. Res., 92*, 6545-6558, 1987.

Francey, R. J., F. J. Robbins, C. E. Allison, and N.G. Richards, The CSIRO global survey of CO_2 stable isotopes, in *Baseline 1988*, edited by S. R. Wilson and G. P. Ayers, 80 pp., Commonwealth Scientific and Industrial Research Organization, Division of Atmospheric Research, Aspendale, Australia, 1990.

Fung, I., K. Prentice, E. Matthews, J. Lerner, and G. Russell, Three-dimensional tracer model study of atmospheric CO_2: Response to seasonal exchanges with the terrestrial biosphere, *J. Geophys. Res., 88*, 1281-1294, 1983.

Fung, I., J. John, J. Lerner, E. Matthews, M. Prather, L. P. Steele, and P. J. Fraser, Three-dimensional model synthesis of the global methane cycle, *J. Geophys. Res., 96*, 12,033-12,065, 1991.

Fushimi, K., Variation of carbon dioxide partial pressure in the western North Pacific surface water during the 1982/83 El Niño event, *Tellus, 39*(B), 214-227, 1987.

Gaudry, A., P. Monfray, G. Polian, and G. Lambert, The 1982-1983 El Niño: A 6 billion ton CO_2 release, *Tellus, 39*(B), 209-213, 1987.

Halpert, M. S., C. F. Ropelewski, T. R. Karl, J. K. Angell, L. L. Stowe, R. R. Heim, A. J. Miller, and D. R. Rodenhuis, 1992 brings return to moderate global temperatures, *Eos Trans. AGU, 74(38)*, 433-439, 1993.

Hobbs, P. V., and L. F. Radke, Airborne studies of the smoke from the Kuwait oil fires, *Science, 256*, 987-991, 1992.

Hogan, K. B., J. S. Hoffman, and A. M. Thompson, Methane on the greenhouse agenda, *Nature, 354*, 181-182, 1991.

Intergovernmental Panel on Climate Change (IPCC), Climate Change, *The IPCC Scientific Assessment*, 365 pp., Cambridge University Press, New York, 1990.

Keeling, C. D., T. P. Whorf, C. S. Wong, and R. D. Bellegay, The concentration of atmospheric carbon dioxide at Ocean Weather Station P from 1969 to 1981, *J. Geophys. Res., 90*, 10,511-10,528, 1985.

Keeling, C. D., S. C. Piper, and M. Heimann, A three-dimensional model of atmospheric CO_2 transport based on observed winds, 4, Mean annual gradients and interannual variations, in *Aspects of Climate Variability in the Pacific and the Western Americas, Geophys. Monogr. 55*, edited by D. H. Peterson, 363 pp, AGU, Washington, D. C., 1989a.

Keeling, C. D., R. B. Bacastow, A. F. Carter, S. C. Piper, T. P. Whorf, M. Heimann, W. G. Mook, and H. Roeloffzen, A three-dimensional model of atmospheric CO_2 transport based on observed winds, 1, Analysis of observational data, in *Aspects of Climate Variability in the Pacific and the Western Americas, Geophys. Monogr. 55*, edited by D.H. Peterson, 363 pp., AGU, Washington, D. C., 1989b.

Komhyr, W. D., L. S. Waterman, and W .R. Taylor, Semiautomatic nondispersive infrared analyzer apparatus for CO_2 air sample analyses, *J. Geophys. Res., 88*, 1315-1322, 1983.

Komhyr, W. D., R. H. Gammon, T. B. Harris, L. S. Waterman, T. J. Conway, W. R. Taylor, and K. W. Thoning, Global atmospheric CO_2 distribution and variations from 1968-82 NOAA/GMCC CO_2 flask sample data, *J. Geophys. Res., 90*, 5567-5596, 1985.

Mahlman, J. D., and W. J. Moxim, Tracer simulation using a global general circulation model: Results from a mid-latitude instantaneous source experiment, *J. Atmos. Sci., 35*, 1340-1374, 1978.

Manning, M. R., Seasonal cycles in atmospheric CO_2 concentrations, in *The Global Carbon Cycle: Proceedings of the NATO Advanced Study Institute on the Contemporary Carbon Cycle at Il Ciocco, Italy*, edited by M. Heimann, pp. 65-94, Springer-Verlag, New York, 1993.

Marland, G., and T. Boden, CO_2 emissions-modern record, in *Trends '91: A Compendium of Data on Global Change*, edited by T.A. Boden, R.J. Sepanski, and F.W. Stoss, 665 pp., Carbon Dioxide Information Analysis Center, Oak Ridge National Laboratory, Oak Ridge, Tenn., 1991.

Nakazawa, T., S. Morimoto, S. Aoki, and M. Tanaka, Time and space variations of the carbon isotopic ratio of tropospheric carbon dioxide over Japan, *Tellus, 45*(B), 258-274, 1993.

Novelli, P. C., L. P. Steele, and P. P. Tans, Mixing ratios of carbon monoxide in the troposphere, *J. Geophys. Res., 97*, 20,731-20,750, 1992.

Pearman, G., and P. Hyson, Activities of the global biosphere as reflected in atmospheric CO_2 records, *J. Geophys. Res., 85*, 4457-4467, 1980.

Pearman, G. I., and P. Hyson, Global transport and inter-reservoir exchange of carbon dioxide with particular reference to stable isotopic distributions, *J. Atmos. Chem., 4*, 81-124, 1986.

Plumb, R. A., and J. D. Mahlman, The zonally averaged transport characteristics of the GFDL general circulation/transport model, *J. Atmos. Sci., 44*, 298-327, 1987.

Potter, C .S., J. T. Randerson, C. B. Field, P. A. Matson, P. M. Vitousek, H. A. Mooney, and S. A. Klooster, Terrestrial ecosystem production: A process model based on global satellite and surface data, *Global Biogeochem. Cycles, 7*, 811-841, 1993.

Research Systems Incorporated, *IDL Users Guide*, Interactive Data Language, Boulder, Colorado, 1991.

Reynolds, R. W., and D. C. Marsico, An improved real-time global sea surface temperature analysis, *J. Clim., 6*, 114-119, 1993.

Robertson, J. E., and A. J. Watson, Thermal skin effect of the surface ocean and its implications for CO_2 uptake, *Nature, 358*, 738-740, 1992.

Sarmiento, J. L., and E. T. Sundquist, Revised budget for the oceanic uptake of anthropogenic carbon dioxide, *Nature, 356*, 589-593, 1992.

Steele, L. P., P. J. Fraser, R. A. Rasmussen, M. A. K. Khalil, T. J. Conway, A. J. Crawford, R. H. Gammon, K. A. Masarie, and K. W. Thoning, The global distribution of methane in the troposphere, *J. Atmos. Chem., 5*, 125-171, 1987.

Steele, L. P., E. J. Dlugokencky, P. M. Lang, P. P. Tans, R. C. Martin, and K. A. Masarie, Slowing down of the global accumulation of atmospheric methane during the 1980's, *Nature, 358*, 313-316, 1992.

Tans, P. P., T. J. Conway, and T. Nakazawa, Latitudinal distribution of the sources and sinks of atmospheric carbon dioxide derived from surface observations and an atmospheric transport model, *J. Geophys. Res., 94*, 5151-5172, 1989.

Tans, P. P., I. Y. Fung, and T. Takahashi, Observational constraints on the global atmospheric CO_2 budget, *Science, 247*, 1431-1438, 1990.

Tans, P. P., I. Y. Fung, and I. G. Enting, Storage versus flux budgets: The terrestrial uptake of CO_2 during the 1980's, in *Biotic Feedbacks in the Global Climate System: Will the Warming Feed the Warming?*, edited by G.M. Woodwell and F.T. Mackenzie, Oxford University Press, New York, in press, 1994.

Thompson, M. L., I. G. Enting, G. I. Pearman, and P. Hyson, Interannual variations of atmospheric CO_2 concentration, *J. Atmos. Chem., 4*, 125-155, 1986.

Thoning, K. W., P. Tans, T. J. Conway, and L. S. Waterman, NOAA/GMCC calibrations of CO_2-in-air reference gases: 1979-85, *NOAA Tech. Memo, ERL ARL-150*, 63 pp., Environ. Res. Lab., Boulder, Colo., 1987.

Thoning, K. W., P. P. Tans, and W. D. Komhyr, Atmospheric carbon dioxide at Mauna Loa Observatory, 2, Analysis of the NOAA GMCC data, 1974-1985, *J. Geophys. Res., 94*, 8549-8565, 1989.

Townsend, A. R., P. M. Vitousek, E. A. Holland, Tropical soils could dominate the short-term carbon cycle feedbacks to increased global temperatures, *Clim. Change, 22*, 293-303, 1992.

T. J. Conway, P. P. Tans, K. W. Thoning, and L. S. Waterman, NOAA Climate Monitoring and Diagnostic Laboratory, 325 Broadway, Boulder, CO 80303.

D. R. Kitzis, K. A. Masarie, and N. Zhang, Cooperative Institute for Research in Environmental Sciences, University of Colorado, Boulder, CO 80302.

(Received February 15, 1994; revised July 25, 1994;
accepted July 25, 1994.)